Boise State University

ScholarWorks

Physics Faculty Publications and Presentations   Department of Physics

Strain-Driven Quantum Dot Self-Assembly by Molecular Beam Epitaxy

Kathryn E. Sautter
Boise State University

Kevin D. Vallejo
Boise State University

Paul J. Simmonds
Boise State University

Strain-driven quantum dot self-assembly by molecular beam epitaxy

Kathryn E. Sautter,[1] (iD) Kevin D. Vallejo,[1] (iD) and Paul J. Simmonds[1,2,a)] (iD)

AFFILIATIONS

[1]Micron School of Materials Science and Engineering, Boise State University, 1910 University Drive, Boise, Idaho 83725, USA
[2]Department of Physics, Boise State University, 1910 University Drive, Boise, Idaho 83725, USA

Note: This paper is part of the special collection on Materials for Quantum Technologies: Computing, Information, and Sensing.
[a)]**Author to whom correspondence should be addressed:** paulsimmonds@boisestate.edu

ABSTRACT

Research into self-assembled semiconductor quantum dots (QDs) has helped advance numerous optoelectronic applications, ranging from solid-state lighting to photodetectors. By carefully controlling molecular beam epitaxy (MBE) growth parameters, we can readily tune QD light absorption and emission properties to access a broad portion of the electromagnetic spectrum. Although this field is now sufficiently mature that QDs are found in consumer electronics, research efforts continue to expand into new areas. By manipulating MBE growth conditions and exploring new combinations of materials, substrate orientations, and the sign of strain, a wealth of opportunities exist for synthesizing novel QD nanostructures with hitherto unavailable properties. As such, QDs are uniquely well positioned to make critical contributions to the development of future quantum technologies. In this tutorial, we summarize the history of self-assembled QDs, outline some examples of quantum optics applications based on QDs, discuss the science that explains the spontaneous formation of QDs, and provide recipes for successful QD growth by MBE for some of the most commonly used semiconductor materials systems. We hope that compiling this information in one place will be useful both for those new to QD self-assembly and for experienced researchers, ideally supporting the community's efforts to continue pushing the boundaries of knowledge in this important field.

I. INTRODUCTION AND BACKGROUND

For the last 30 years, epitaxial quantum dots (QDs) have been the subject of intense research interest across physics, materials science, and electrical engineering. QDs represent a highly tunable platform for research driven by fundamental scientific questions and technological applications alike. We can think of a QD as a quantum well that confines charge carriers in all three spatial dimensions. When the size of the QD approaches the electron's de Broglie wavelength, the resulting energy quantization produces a density of states that approximates a series of discrete delta functions. Viewed from this perspective, the quantum states of an individual QD are very similar to the electron orbitals of an atom. The key difference is that an atom's position in the periodic table dictates the specific energies of its electron orbitals. In contrast, the confined energy states of a QD are inherently tunable. By controlling their size, we can design and create QDs that emit or absorb light at very specific wavelengths.

In the 1970s, researchers used a new technology, molecular beam epitaxy (MBE),[1] to synthesize the first quantum wells with one-dimensional quantum confinement.[2,3] However, going further, to produce nanostructures that offered two-dimensional or three-dimensional quantum confinement was, at the time, a huge technological challenge. By the early 1990s, researchers had developed two techniques for achieving three-dimensional confinement, both based on the initial growth of a quantum well.

The first approach used top-down processing to fabricate narrow pillars with diameters of a few tens of nanometers. Each pillar contained a small disc of the quantum well, with in-plane confinement offered by the pillar's sidewalls [Fig. 1(a)].[4,5] Indeed, this was the approach used in the paper that coined the term "quantum dots" to describe nanostructures with three-dimensional confinement.[6]

The second approach grew out of quantum point contact research,[7–10] where electrostatic gates on the sample surface lower
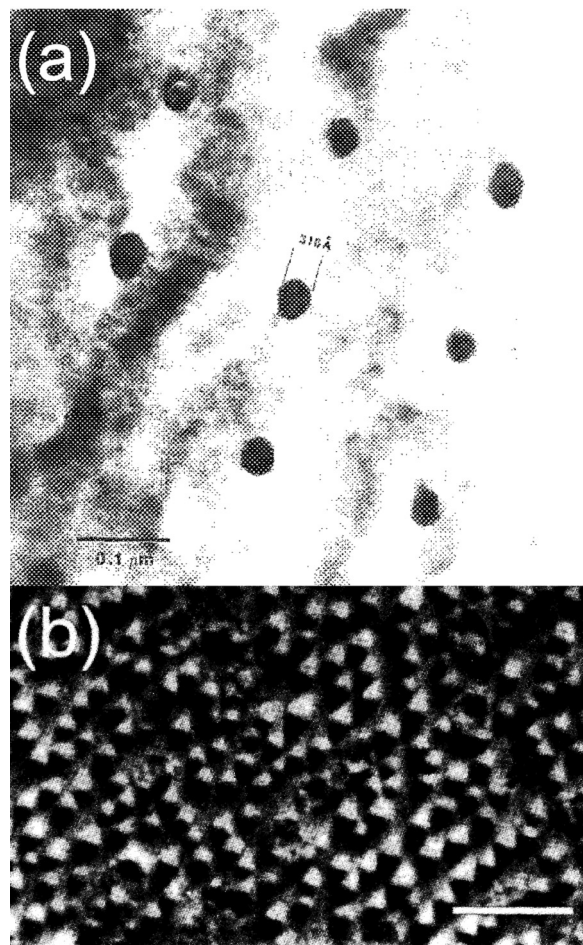
FIG. 1. (a) Transmission electron microscope (TEM) image showing early examples of QDs created by electron beam lithography and ion beam milling. The average width of these InGaAs/InP QDs is ∼30 nm. Reprinted with permission from Temkin *et al.*, Appl. Phys. Lett. **50**, 413–415 (1987). Copyright 1987 AIP Publishing LLC.[5] (b) Plan-view TEM image of self-assembled InAs QDs in a GaAs matrix (scalebar = 100 nm). Reprinted with permission from Grundmann *et al.*, Phys. Rev. Lett. **74**, 4043 (1995). Copyright 1995 American Physical Society.[14]

the Fermi level to deplete carriers from specific regions of the underlying quantum well. In this way, researchers produced small, discrete disks or "puddles" within the quantum well, each of which offered three-dimensional confinement.[11–13]

These two approaches both permit the synthesis of arrays of QDs at precise locations, making it easy to subsequently build devices around them. One can also tune the diameter of gate-defined QDs after fabrication, simply by controlling the gate voltage applied. These approaches do, however, share some disadvantages. Both require extensive post-growth processing, which can be expensive and time-consuming. What is more, the maximum areal QD density that can be practically achieved with these

approaches is ∼10^8 cm^{-2}, which is lower than the >10^{10} cm^{-2} needed for efficient QD-based light emitters.

The discovery of self-assembled QDs around 1990 presented researchers with a straightforward synthesis approach for QDs that required no post-growth processing and could easily provide areal densities >10^{10} cm^{-2} [Fig. 1(b)]. The development of self-assembled QDs came about almost by accident. Since the early 1980s, researchers had known that certain combinations of materials began growth in a smooth, layer-by-layer growth mode. However, once some critical thickness was reached, a spontaneous transition to 3D island formation occurred, consistent with the Stranski–Krastanov (SK) growth mode.[15,16] Island growth was typically associated with materials systems such as Ge on Si(001) and In$_x$Ga$_{1-x}$As on GaAs(001) that have large differences in lattice constants and/or surface energies.[15–17] Considerable efforts were invested in understanding and suppressing the self-assembly of these undesirable 3D islands.[18–22]

The breakthrough came when researchers recognized first that during the initial stages of growth, these 3D islands are actually dislocation-free,[22–25] and second that their heights and diameters are close to the electron de Broglie wavelength in these semiconductors.[26,27] When islands consisting of a narrow bandgap semiconductor were embedded within a wider bandgap semiconductor, they behaved as optically active QDs.[14,27–31] Carrier confinement in quantized energy states was confirmed using photoluminescence (PL) spectroscopy.[32–35]

Once these facts were established, the floodgates opened, and self-assembled QDs became the subject of intense research activity. Self-assembled QDs have since been demonstrated in a range of materials systems, including Ge/Si, In$_x$Ga$_{1-x}$As/GaAs, In$_x$Ga$_{1-x}$Sb/GaAs,[36,37] In$_x$Ga$_{1-x}$P/GaAs,[38–40] InAs/InP,[41–43] In$_x$Ga$_{1-x}$As/GaP,[38,44] GaN on AlN,[45,46] In$_x$Ga$_{1-x}$N on GaN,[47,48] CdSe on ZnSe,[49,50] and CdTe on ZnTe.[51,52] The features that unite all of these materials systems are growth on a (001)-oriented substrate and the presence of compressive strain.

More recently, QDs on (110)- and (111)-oriented surfaces have also been achieved by using tensile rather than compressive strain to drive the self-assembly process.[53–60] Tensile-strained self-assembly has now been demonstrated in the GaP/GaAs, GaAs/In$_{0.52}$Al$_{0.48}$As, and Ge/In$_{0.52}$Al$_{0.48}$As materials systems on both (110) and (111) substrate orientations.

Compressive strain increases a semiconductor's bandgap, while tensile strain reduces it.[61] In conjunction with the size of the bulk bandgap and quantum size effects, we can, therefore, use the sign and magnitude of strain in a QD to achieve exquisite control over the transition energy between electron and hole ground states. Together with their discrete density of states, these characteristics mean that laser diodes built around QDs exhibit exceptionally low-threshold currents and excellent temperature stability.[62–64] QDs will continue to drive innovations in optoelectronic research.

II. QUANTUM DOTS FOR QUANTUM TECHNOLOGIES

It is the unique properties of QDs for quantum information and communication applications that is of most relevance to this special topic collection.[58,65–68] QDs are ideally suited for use as single-photon emitters, as single-photon detectors, and as sources

of entangled photons, all of which are key components in various quantum information systems.[65,67–72]

A. QD single-photon emitters

An electron and a hole confined within a single QD will experience electrostatic attraction and can form a bound state known as an exciton. When the electron recombines with the hole, a photon is emitted whose energy corresponds to the transition between the electron and hole ground states of the QD. We can create excitons in a QD device structure by either optical or electrical means. Since one exciton can only produce one photon, we can, therefore, use a QD to generate single photons on demand.[73] A QD placed within an optical cavity, such as a photonic crystal, can hence be used as an efficient single-photon emitter.[72,74,75]

We use photon correlation measurements to verify that a QD is indeed behaving as a quantum emitter of single photons. Quantum emitters exhibit a property known as photon antibunching, which means that the probability of more than one photon being emitted within some time window is essentially zero.[77,78] In other words, a QD that is truly a quantum light source can only emit a single photon at a time. To check for photon antibunching, we use a Hanbury Brown and Twiss (HBT) setup.[79] Using a monochromator, we spectrally filter the QD emission and then pass it through a non-polarizing 50:50 beam splitter. Each arm goes to a high-sensitivity, low-noise single-photon detector. These two detectors are connected to a timer whose resolution is typically a few 100s of picoseconds. This timer provides the delay time (τ) between successive photon detection events, allowing one to plot the second-order autocorrelation function $g^{(2)}(\tau)$.[76] Photon antibunching, and hence single-photon emission from a QD, is characterized by a dip in the second-order autocorrelation function at zero time delay, where $g^{(2)}(0) < 0.5$ (Fig. 2). Using pulsed laser
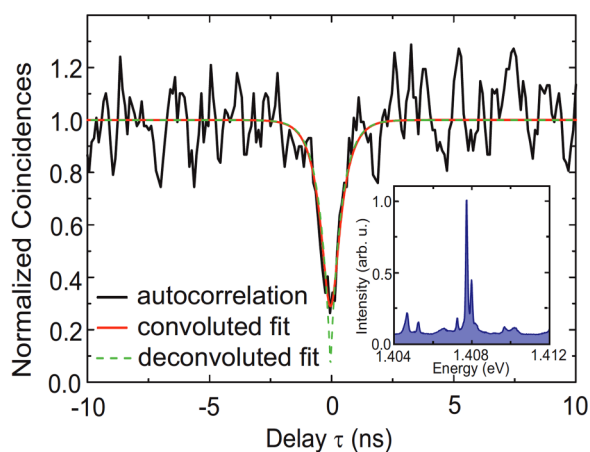

FIG. 2. Autocorrelation of a QD emission line shown in the inset. The dip at $\tau \sim 0$ ns extends below 0.5 confirming single-photon emission. The dashed line shows a deconvoluted fit to these data from which a value of $g^{(2)}(0) = 0.05^{+0.17}_{-0.05}$ is extracted. Reprinted with permission from Unsleber *et al.*, Opt. Express **24**, 23198–23206 (2016). Copyright 2016 The Optical Society.[76]

excitation, we can use this approach to demonstrate triggered single-photon emission.[73,76,78]

High-quality single-photon emitters are in great demand for various quantum technologies,[71] including quantum key distribution (QKD),[65,80] true random number generation,[81] and quantum metrology for sensing below the shot-noise limit.[82]

B. QD single-photon detectors

The ability to detect single photons is clearly central to the HBT setup described above for confirming single-photon emission. However, single-photon detection is also critical in its own right to the success of various quantum technologies, perhaps most notably for QKD applications.[69,83]

Although single-photon detectors based on Si avalanche photodiodes (APDs) and superconducting nanowires are in widespread use,[71,84–86] QD-based single-photon detectors offer several advantages.[85,87–92] These include a III–V semiconductor device architecture compatible with QD single-photon emitters, infrared detection beyond the band edge of Si (for example, at fiber-optic wavelengths), very low dark count rates, and the lack of problems with afterpulse noise seen in InGaAs APDs that result from the avalanche process.[85,87–92]

For single-photon detection, QDs are placed close to the channel of a field-effect transistor[88,89,91] or the double barriers of a resonant tunneling diode.[90,92,93] The capture of a single photon by a QD generates an electron–hole pair, which in turn produces a measurable change in the device current, and the single photon is detected.

C. QD entangled photon sources

According to quantum mechanics, a pair of quantum entangled photons exhibits a superposition of all polarization states and can be described by a single wavefunction. These entangled photons exhibit the counterintuitive property that even if some arbitrarily large distance separates them, their polarizations remain physically linked. Measuring the polarization of one photon instantaneously causes its counterpart to assume the opposite polarization. Entangled photons are essential for various quantum communication technologies.[68,70,94,95] As a result, research groups have explored various means to create entangled photons, including non-linear optical effects, single atoms or atomic ensembles, and nitrogen color vacancies in diamond.[96–100] However, the generation of entangled photon pairs in semiconductor QDs has some distinct advantages. As we have seen, QDs are compact, tunable, and we can electrically trigger them to emit photons on-demand.[73,101,102]

We can use a QD to generate entangled photons via the biexciton–exciton cascade (Fig. 3).[103–105] Two electrons and two holes within a QD form a bound biexciton state $|XX\rangle$. For the biexciton to decay to the ground state $|0\rangle$, the two electron–hole pairs must recombine, releasing two photons in the process. The key is that the first exciton recombination event puts the remaining exciton in one of two states, $|X_H\rangle$ or $|X_V\rangle$, which are orthogonally polarized. If we cannot say which of the two intermediate exciton states the cascade passed through, then the polarization of the two photons emitted will be entangled.
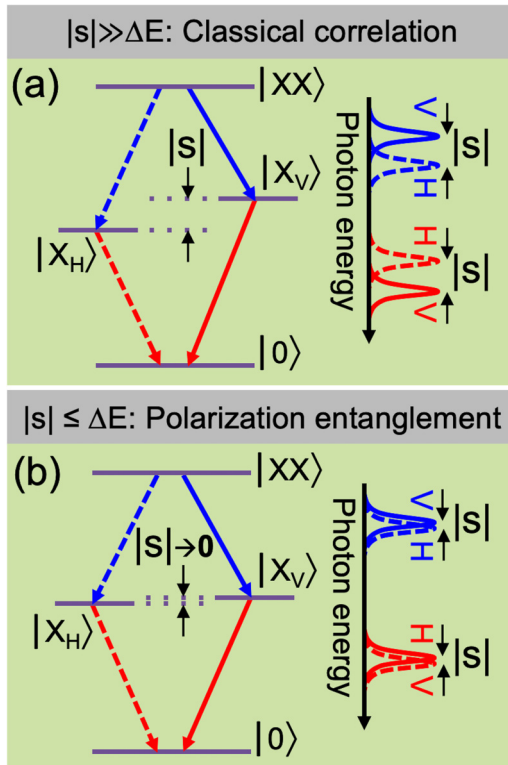
FIG. 3. Biexciton–exciton cascades with corresponding photon emission spectra. (a) For large fine-structure splitting $|s|$, the two decay paths are distinguishable, leading to classically correlated photon polarizations. (b) As $|s| \to 0$, the two paths become indistinguishable and emitted photons are polarization entangled (after Ref. 105).

The key to remaining ignorant of this "which-path" information, and so to obtaining entangled photons, is the difference in energy $|s|$ between the two intermediate exciton states. When $|s|$, referred to as the fine-structure splitting, is larger than the radiative homogeneous linewidth (ΔE), we can distinguish between the two decay paths, destroying the entanglement [Fig. 3(a)]. However, when $|s|$ is reduced, ideally to zero so that $|X_H\rangle$ and $|X_V\rangle$ are degenerate, then the two decay paths are indistinguishable, and the two emitted photons will be polarization entangled [Fig. 3(b)]. Testing for photon entanglement involves polarization-resolved second-order cross-correlation measurements using an HBT setup with rotatable $\lambda/2$ and $\lambda/4$ plates. In this way, one can populate the two-photon density matrix, where strong off-diagonal elements signify photon entanglement.[103,105]

In practice, however, synthesizing QDs with $|s| \sim 0$ is not trivial. Self-assembled QDs grown on the traditional (001) surface suffer from structural anisotropy and piezoelectric effects[66] so that $|s|$ can be tens or hundreds of μeV.[106,107] However, various techniques, including thermal, electrical, and magnetic tuning, enable researchers to systematically reduce $|s|$ to zero.[103,106,108,109] In this way, entangled-photon light-emitting diodes (LEDs) have been demonstrated.[110,111]

An alternative approach is to choose a QD system that has an instrinsically low fine-structure splitting. Self-assembled QDs grown on (111)-oriented substrates exhibit vanishingly small values of $|s|$ due to the high symmetry of this surface.[66] QD formation on (111) surfaces can be achieved with either droplet epitaxy (see Sec. III) or tensile-strained self-assembly (see Sec. VI), with both methods showing promise for future quantum technology applications.[58,112]

In the remainder of this tutorial, we seek to provide an overview of the fundamental principles and techniques relating to the growth of self-assembled QDs by MBE. Clearly, an exhaustive review of every study of self-assembled QDs is beyond the scope of this tutorial. Rather, we have aimed to summarize the typical MBE parameters widely used to grow QDs in some of the more commonly encountered QD materials systems. It is our hope that this information will be sufficient for someone unfamiliar with QD self-assembly to get started and to begin growing optically active QDs by MBE for quantum information applications.

III. APPROACHES TO QD GROWTH BY MBE

The technological potential of QDs quickly pushed research toward the phenomenological design of processes that produce uniform, high-density, defect-free QD arrays. For device applications, the ability to reliably tailor QD size, shape, and spacing was essential. QD self-assembly meets these requirements without the need for pre-growth substrate patterning and can be accomplished in two ways: via induced nucleation through droplet epitaxy[113] or through strain-driven processes, which are the focus of this tutorial.[114] These techniques rely on stochastic nucleation events so that the resulting self-assembled QDs are distributed randomly across the substrate. For an excellent review of efforts to engineer QD arrays with specific placement, see Ref. 115.

Droplet epitaxy (DE) enables the growth of QDs, even in unstrained materials systems.[113,116,117] DE growth of III–V QDs is a three-step process. (1) Grow a smooth III–V buffer surface and close the group V source(s) and wait for the background pressure to become negligibly low. (2) Open the group III source(s) to deposit a few monolayers of pure metal to form liquid nanodroplets. (3) Reopen the group V source(s), crystallizing the liquid nanodroplets into III–V semiconductor QDs. By removing the requirement for strain, this method increases the possible combinations of materials from which we can synthesize QDs.[118] Researchers have also grown QD molecules, quantum rings, and quantum holes by DE.[118–120] References 121 and 122 provide more information on DE. The rest of this tutorial concentrates solely on the self-assembly of strained QDs.

IV. STRAIN-DRIVEN QD SELF-ASSEMBLY

A. Thermodynamics and kinetics in MBE

As with other epitaxial growth techniques, MBE depends on thermodynamic and kinetic contributions. The rates of various processes, the strain in a given material system, and the relative magnitudes of the surface energies are all critical factors in determining the outcome of a given growth. Researchers use thermodynamic wetting arguments to explain and predict the growth mode

for a given material system.[123–125] The three relevant parameters are the surface free energies of the epilayer–vacuum interface γ_e, the epilayer–substrate interface γ_i, and the substrate–vacuum interface γ_s. In addition, if the epilayer's lattice constant is larger (smaller) than that of the substrate, the epilayer will experience compressive (tensile) strain due to the Poisson effect.[126]

Classifying growth modes based solely on surface energy and strain considerations is valid only if we assume the system is close to thermodynamic equilibrium. MBE is a far-from-equilibrium growth technique,[124] although annealing can provide sufficient time for effects such as Ostwald ripening to occur, where larger QDs grow at the expense of smaller QDs.[127] Whether growth occurs or not is also a function of the relevant rates of various processes including atomic arrival, desorption, diffusion, and bonding. There are numerous interactions between adatoms and terraces, steps, kinks, and surface defects (Fig. 4). At typical atomic fluxes and substrate temperatures, growth by MBE is, therefore, limited by kinetics rather than thermodynamics.

During MBE, the interplay between thermodynamics and kinetics gives rise to three growth modes. First is the Frank–van der Merwe (FM) growth mode, which proceeds either via 2D layer-by-layer [Fig. 4(a)] or step-flow crystal growth [Fig. 4(b)]. On
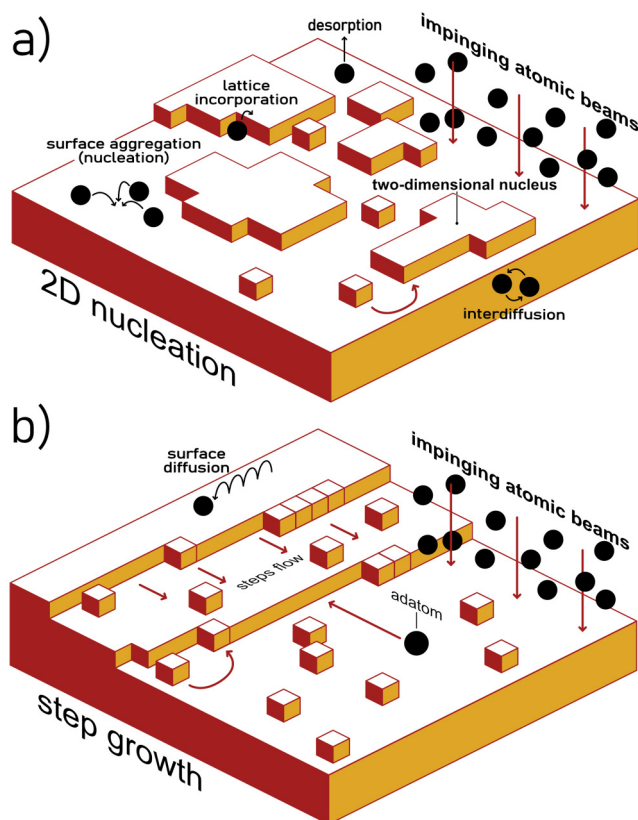

FIG. 4. Kinetic processes present during the nucleation and growth of 2D thin films via (a) layer-by-layer growth and (b) step-flow growth.

surfaces where the average adatom diffusion length is less than the distance between neighboring step-edges, crystal growth will tend to proceed via layer-by-layer growth. On surfaces where the average adatom diffusion length is greater than the distance between neighboring step-edges, crystal growth will tend to proceed via step-flow growth.

During layer-by-layer growth, low mobility adatoms will locally nucleate into 2D islands that eventually merge to form complete single-crystal layers [Fig. 4(a)].[128] If adatom diffusion is very low (for example, if the substrate temperature is too low), multilayer growth (i.e., roughening) can occur. Adatoms landing on top of existing 2D islands have insufficient energy to overcome the Ehrlich–Schwoebel (ES) barrier and descend to the main epitaxial surface. ES potential barriers exist at the top of step-edges and prevent low energy adatoms from moving down to the terrace below.[129] The ES barrier occurs because as the adatom passes over the top of the step-edge, it sees a "missing" atom and so it has fewer bonding sites (has lower coordination) than an adatom on the smooth terrace. The result of the ES barrier is that low energy adatoms may coalesce to form a new island on top of an existing island before the full 2D layer is completed.[123]

In contrast, for high mobility adatoms whose diffusion lengths exceed the average terrace width, step-flow growth may occur instead [Fig. 4(b)]. An adatom on the lower terrace that is able to reach the bottom of a step-edge will encounter a potential well.[129] This potential well occurs because of the increase in adatom coordination due to the opportunity for bonding with step-edge atoms as well as those on the terrace itself. The result of this potential well is that most adatoms will join the growing crystal at the step-edges [Fig. 4(b)]. The step-edges grow out at the same rate and the surface morphology is essentially preserved.

For more detail on ES barriers, and crystal growth kinetics in general, we direct the reader to Refs. 130 and 131.

FM growth typically occurs in materials systems where strain is low. When $\gamma_e + \gamma_i < \gamma_s$, it is energetically favorable for the epilayer to completely wet the substrate surface, giving rise to the FM growth mode [Fig. 5(a)]. It follows that the spontaneous formation of 3D QDs does not arise naturally from this growth mode.

B. Volmer–Weber growth

The second growth mode we must consider is the Volmer–Weber (VW) growth mode, which produces discrete, 3D islands [Fig. 5(b)]. For VW growth, the condition $\gamma_e + \gamma_i > \gamma_s$ must be met, resulting in dewetting of the epilayer so that 3D islanding occurs. In situations close to thermodynamic equilibrium, the contact angle between the VW islands and the substrate surface is given by $\cos\theta = (\gamma_s - \gamma_i)/\gamma_e$.[123] In practice, the VW growth mode is rarely encountered among the semiconductors of interest for QD-based optoelectronics. Typically, only very thin layers of materials under extremely high strains (>10%) self-assemble via the VW growth mode, for example, in the InPSb/InP, GaPSb/GaP, and InN/GaN QD systems.[132–134]

That being said, QD self-assembly by the VW mode does occur under lower strains in some hybrid group V/III–V semiconductor systems.[135–140] VW-based self-assembly has also been reported for tensile-strained systems such as GaP/GaAs(110) and
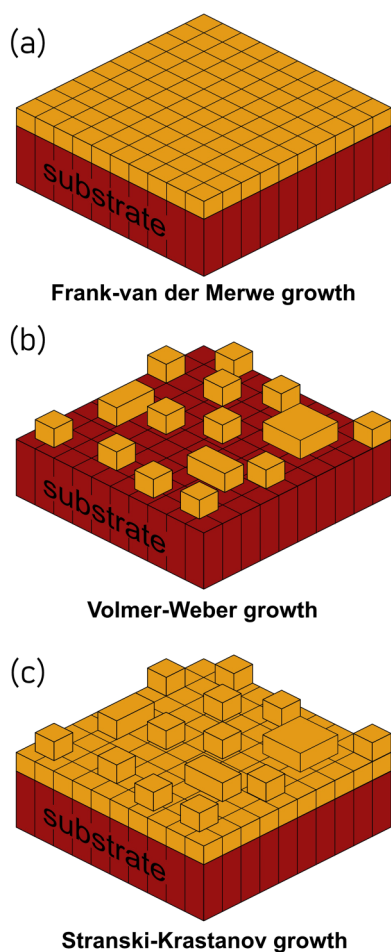
FIG. 5. Different growth modes during MBE growth resulting from a thermodynamic interaction of surface energies: (a) the FM layer-by-layer growth mode, (b) the Volmer–Weber (VW) growth mode, which produces 3D islands directly on a substrate; and (c) the SK growth mode in which 3D islands form on top of a complete 2D wetting layer.

FIG. 6. Atomic force microscope (AFM) image of tensile Ge/InAlAs(111)A QDs that self-assemble via the VW growth mode. Most of the Ge QDs form at the step-edges of the InAlAs surface.

Ge/InAlAs(111)A, where QD formation is mediated by step-edges on the substrate surface.[53,139] If the potential well associated with the ES barrier is sufficiently deep, adatoms will not cross from one terrace to another but instead preferentially accumulate at the bottom of the step-edges.[53] This means that locally, the adatom density can quickly become high enough to trigger island nucleation, even when the total amount of material deposited is ≪1 monolayer. The result is the preferential self-assembly of QDs at the step-edges [Fig. 6], in contrast to the randomly distributed QDs we typically see during strain-driven self-assembly.

C. Stranski–Krastanov growth

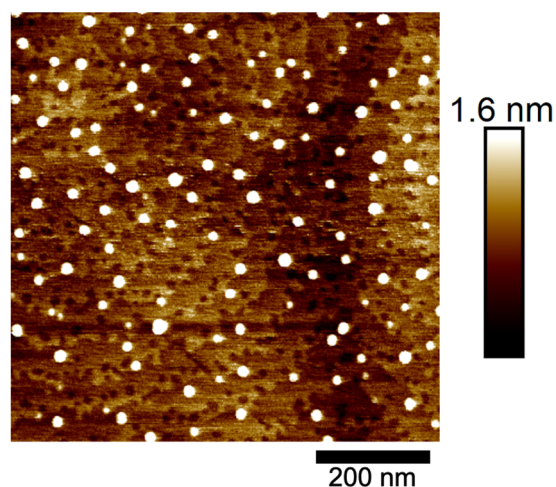The third growth mode we must consider is the Stranski–Krastanov (SK) growth mode, where initial 2D growth transitions into the self-assembly of 3D islands [Fig. 5(c)]. SK growth typically occurs for intermediate levels of compressive or tensile strain, say 2.5%–10%. During the initial stages of SK growth, the various surface free energies are such that the epilayer wets the substrate surface. The group III adatom diffusion length is sufficiently high that we initially obtain layer-by-layer growth of a 2D wetting layer.[142] However, as the wetting layer gets thicker, the strain energy builds up, and a competition between plastic and elastic strain relief mechanisms comes into play.[55,143] Depending on the specific combination of sign of strain and substrate orientation, this strain energy will be relieved either plastically by dislocation nucleation and glide, or elastically by surface roughening.[55] For compressive strain on a (001) substrate or tensile strain on a (110) or (111) substrate, elastic strain relief is energetically favorable, and a morphological change can occur from 2D to 3D growth. This transition is the hallmark of the SK growth mode.

Due to its propensity to surface segregate, the presence of indium in certain QD systems can further complicate the picture. The archetypal example of this is in the self-assembly of InGaAs/GaAs(001) QDs. In–Ga intermixing at the epilayer–substrate interface dilutes the indium composition of the InGaAs epilayer below its nominal value (Fig. 10).[144,145] However, indium also undergoes strain-driven vertical segregation, which enriches indium content at the InGaAs surface.[144] Once this surface indium concentration reaches 80%–85%,[144] the strain is large enough for the SK transition from 2D to 3D growth to occur.[143,146] As we reduce the nominal indium composition of the deposited InGaAs, we lower the strain, but we also lower the amount of indium available. This means that the wetting layer will grow thicker before this critical surface indium concentration is achieved, and self-assembly begins.

It is interesting to note that reversing the situation, so that indium is present in the matrix material but not in the QDs, can lead to some unusual effects such as SK growth with a tunable wetting layer thickness (see Sec. VI A).[60]

Once the critical thickness has been reached, SK growth proceeds via the formation of discrete 3D islands on top of the 2D wetting layer. As discussed above, either compressive or tensile strain can be used to drive SK growth as long as a substrate with the correct crystallographic orientation is used: [compressive + (001); tensile + (111)or (110)].[55,59,60,142] For these specific combinations, the resulting 3D islands will be elastically strained and free from dislocations, provided the total amount of material deposited is less than some maximum amount, typically a few monolayers (ML). Exceeding this maximum will allow the accumulated strain energy in the wetting layer and QDs to overcome the energy barrier to dislocation nucleation, and plastic strain relief will take place.

Although the SK growth mode is much more frequently encountered, we can take advantage of both the SK and VW growth modes to produce 3D self-assembled QDs with high areal densities.[147] Indeed, for Ge QDs grown on InAlAs(111)A (Fig. 6), Sautter *et al.* showed that it may be possible to move between the VW and SK growth modes through careful choice of MBE parameters.[139]

As we have seen, the resulting characteristics of these self-assembled QDs depend on both thermodynamic and kinetic factors, with atomic deposition rate, adsorption, and adatom surface diffusion of particular importance. In the remainder of this tutorial, we look at systems where compressive and tensile strain are the driving forces for the formation of QD self-assembly. Given their much earlier discovery, the body of literature concerning compressively strained QD systems is more extensive and covers a wider variety of materials. In contrast, tensile-strained QDs are still in the comparatively early stages of research but represent a fertile area for the development of novel QD systems.

V. COMPRESSIVELY STRAINED QUANTUM DOTS

Research into epitaxial QDs began with materials systems under compressive strain. Compressive strain occurs when the lattice constant of the QD material is larger than that of the surrounding matrix. Since the lattice constant of most semiconductors relates inversely to their bandgap (Fig. 7), this situation lends itself well to producing quantum confinement of carriers in the QD.

The critical thickness for the SK transition from 2D to 3D growth is dictated by the accumulated compressive strain in the wetting layer. For materials systems under high strain, the critical thickness will, therefore, tend to be lower. For example, InAs/InP QDs (3.2% strain) have a critical thickness of 2.5 ML,[148,149] while InAs/GaAs QDs (7.2% strain) and GaSb/GaAs QDs (7.8% strain) have critical thicknesses of 1.6 ML and 1.2 ML, respectively.[150] As well as driving the self-assembly process, compressive strain has the effect of increasing the semiconductor bandgap [Fig. 8(a)] and hence blue-shifting the light the QDs emit or absorb. In addition, we see that compressive strain breaks the valence band degeneracy, pushing the heavy-hole band above the light-hole band. We can control the strain by changing the composition and hence the lattice constant of the QD and/or the surrounding matrix. In doing so, we can fine-tune the QD band structure, for example, to select light absorption or emission at a specific wavelength. Further tunability is possible by manipulating QD size, shape, and areal density, all of which one can tailor during self-assembled growth by MBE.

The compressively strained materials systems we discuss below represent some of the most widely studied self-assembled QDs, providing an excellent starting point for understanding the newer field of tensile-strained QD self-assembly in Sec. VI.

A. Ge or Ge_xSi_{1-x} on Si(001)

Due to the dominance of Si in the electronics industry, Ge_xSi_{1-x} on Si(001) is one of the most heavily studied diamond-cubic heteroepitaxial systems. By combining the elemental semiconductors Si and Ge, researchers created alloys whose composition allowed them to manipulate both the band structure and, via
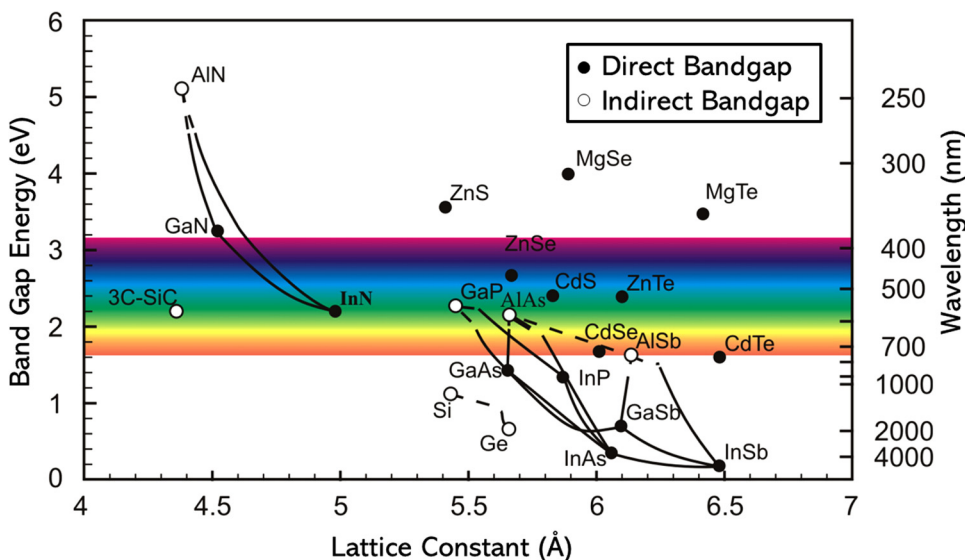
FIG. 7. Room-temperature bandgaps of various elemental and binary compound semiconductors as a function of lattice constant. Reprinted with permission from Fornari, "Epitaxy for energy materials," in *Handbook of Crystal Growth*, 2nd ed., Handbook of Crystal Growth, edited by T. F. Kuech (North-Holland, Boston, 2015), pp. 1–49. Copyright 2015 Elsevier.[141]
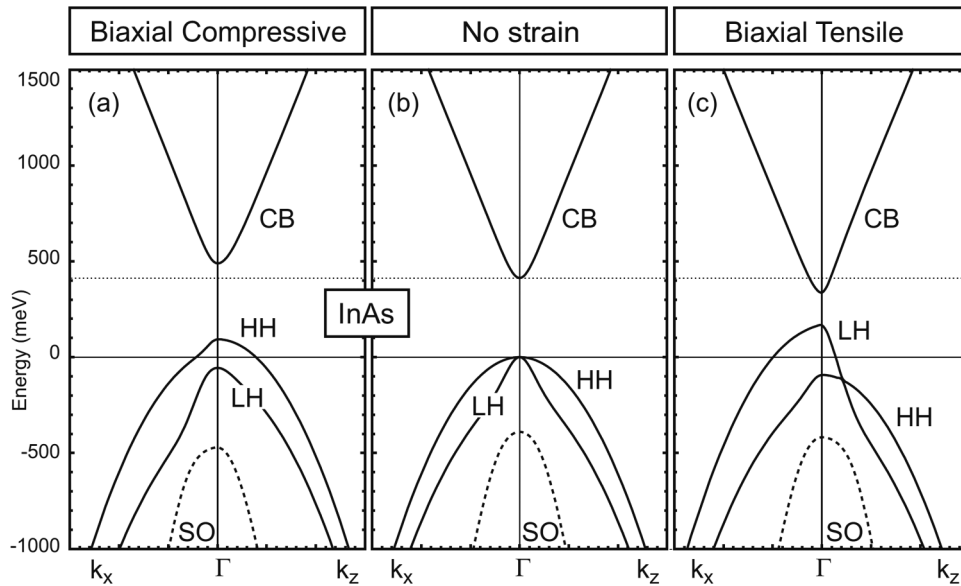
FIG. 8. Calculated band structures for InAs in the presence of (a) biaxial compressive strain, with strain components $\varepsilon_{xx} = \varepsilon_{yy} < 0$ and $\varepsilon_{zz} > 0$, (b) no strain, and (c) biaxial tensile strain, with $\varepsilon_{xx} = \varepsilon_{yy} > 0$ and $\varepsilon_{zz} < 0$. Reprinted with permission from Schliwa *et al.*, "Electronic properties of III-V quantum dots," in *Multi-Band Effective Mass Approximations*, Lecture Notes in Computational Science and Engineering (Springer, Cham, 2014), Vol. 94, pp. 57–85. Copyright 2014 Springer Nature.[151]

lattice constant, the strain (Fig. 7). There is a ~4.2% lattice mismatch between Si and Ge (see Fig. 7).[18,152–154] Not only did strain-relaxed 2D buffers of Ge_xSi_{1-x} alloys lead to important developments in electronic device design,[155,156] they also helped researchers better understand homo- and heteroepitaxy from a kinetic and thermodynamic perspective.

In general, compressively strained Ge_xSi_{1-x} self-assembles into rectangular-based "huts" on Si(001) with {105} facets under typical MBE growth conditions.[152,153,157–159] For further information, several detailed studies of Ge_xSi_{1-x} QD shapes/facets exist.[152,153,157–159] While researchers have explored Ge_xSi_{1-x} self-assembly on Si(001) substrates with a 0°–8° miscut toward the [110] direction,[153,160,161] most studies focus on miscuts of <2°.[153,160,161] Interestingly, exceeding a 4° miscut angle can change the growth mode from SK to VW.[161]

To remove the native oxide before MBE, Si substrates are typically heated to a "flash-clean" temperature of 1050–1255 °C and held there for 40 s[153,157,160,162] or may be first annealed at 900 °C for 3 min before flash-cleaning the Si substrate.[162] The substrate is then cooled to 500–700 °C for Si deposition.[152,154,161–163] At this growth temperature, Si(001) grows with a (2×1) surface reconstruction in a step-flow growth mode.[152] Typical growth rates for Si homoepitaxy are from 0.005 to 0.74 ML/s, with 0.044–0.405 ML/s the most common.[154,161–163] A Si buffer layer of ≥100 nm is grown to act as a bottom potential barrier for the Ge_xSi_{1-x} QDs. The sample may be annealed at 1100 °C for 10 min and then cooled to the desired temperature for Ge_xSi_{1-x} QD growth.[163]

Researchers have demonstrated Ge_xSi_{1-x} QD self-assembly at substrate temperatures from 300 to 750 °C, but 450–600 °C is typical.[24,152–154,157,161–163] The Ge_xSi_{1-x} growth rate can range from 0.0008 to 0.707 ML/s, but we recommend 0.001–0.083 ML/s based on the most common rates in the literature.[24,152,154,157,162,163]

For deposition of pure Ge (i.e., $x = 1$) on Si(001), the wetting layer initially grows via the step-flow mode, with Si/Ge intermixing

at substrate temperatures ≥500 °C.[152,162,163] After 3 ML Ge deposition, the reflection high-energy electron diffraction (RHEED) pattern changes from streaky to spotty, indicative of the SK growth mode transition from 2D growth to 3D island self-assembly.[152–154,157,162,163] For Ge_xSi_{1-x}/Si(001) studies, typical QD deposition amounts are 3–8 ML.[24,152–154,163] Individual layers of Ge_xSi_{1-x} QDs are separated by at least 10 nm of Si and finally capped with ~100 nm of Si to act as the top potential barrier and provide confinement.[24,154]

Surfactants can help delay the SK transition to 3D islanding, thus increasing the critical thickness and red-shifting the energy of the quantum confined states in the wetting layer.[162] Example surfactants are As_4 and Sb_4, with As providing a more stable (i.e., thicker) Ge wetting layer than Sb.[162]

B. $In_xGa_{1-x}As$ on GaAs(001)

As the earliest optically active QD system, self-assembled $In_xGa_{1-x}As$/GaAs(001) QDs are the most extensively studied in the literature. Together with Ge_xSi_{1-x}/Si(001), $In_xGa_{1-x}As$/GaAs(001) QDs gave researchers an opportunity to study MBE growth kinetics and thermodynamics in great detail and opened the door to materials design through strain-engineering. $In_xGa_{1-x}As$/GaAs QD self-assembly is driven by a compressive lattice mismatch of ~7.2% between InAs and GaAs, but despite this large strain, the QDs are free from dislocations.[15,164–167] A direct bandgap (Fig. 8) and strong type-I carrier confinement (Fig. 9), mean that $In_xGa_{1-x}As$/GaAs(001) QDs are well suited to a range of optoelectronic devices.[14]

Here, we describe the MBE conditions most widely used to grow self-assembled $In_xGa_{1-x}As$/GaAs QDs. The native oxide is thermally removed from GaAs(001) substrates under a flux of As_2 or As_4 at anywhere from 580 to 650 °C.[55,166,169,170] A homoepitaxial GaAs(001) buffer of several hundred nanometers is then grown
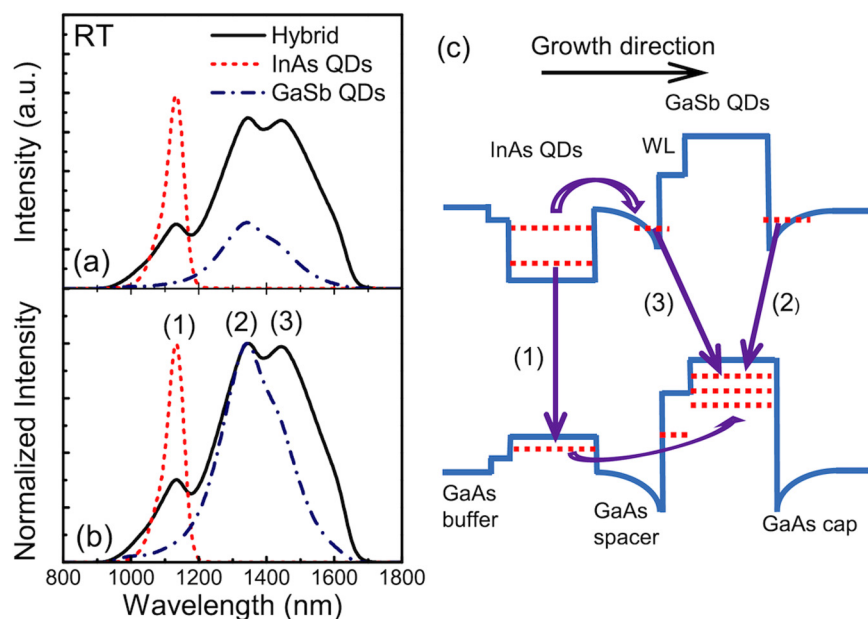
FIG. 9. (a) Room-temperature PL spectra for InAs/GaAs(001) QDs, GaSb/GaAs(001) QDs, and an InAs–GaSb hybrid QD structure. (b) These same spectra normalized to the maximum intensity. (c) The band diagram for this hybrid structure explains the origin of the three peaks and shows the type-I and type-II band alignments of the InAs and GaSb QDs, respectively. Reprinted with permission from Ji *et al.*, Appl. Phys. Lett. **106**, 103104 (2015). Copyright 2015 AIP Publishing LLC.[168]

at a substrate temperature of 550–600 °C (typically closer to 600 °C).[14,26,36,55,119,164,166,168–172] The GaAs growth rate for the buffer is 0.3–1.0 μm/h (often at the higher end of this range).[14,36,55,119,164,166,168–172] GaAs(001) growth typically occurs on the (2 × 4) As-stabilized surface reconstruction, in part because this surface comprises the largest part of the GaAs(001) flux–temperature phase diagram for a given As flux.[26,169,171]

For the growth of binary InAs QDs, the substrate temperature is typically reduced to 400–490 °C.[14,164,166,168,169,173,174] Unless care is taken to reduce the As overpressure during cooling, the GaAs(001) surface will undergo a phase change to the c(4 × 4) surface reconstruction at around 520 °C.[166,171] As a result, most In$_x$Ga$_{1-x}$As/GaAs(001) QDs undergo self-assembly on this c(4 × 4) surface. The In$_x$Ga$_{1-x}$As is deposited at 0.018–0.3 ML/s, and typical deposition amounts range from 1.4 to 2.7 ML.[14,166–169,171,173]

Once the InAs critical wetting layer thickness of 1.6–1.7 ML is reached, the RHEED pattern rapidly changes. Consistent with the SK transition from 2D to 3D growth, the streaky c(4 × 4) pattern of the wetting layer gives way to a spotty pattern, with spots and chevrons forming along the [110] and [$\bar{1}$10] azimuths, respectively.[14,167,168,171] The result of this step is the self-assembly of InAs QDs. Cation intermixing naturally occurs at the InAs–GaAs interface to form an In$_x$Ga$_{1-x}$As alloy.[26,144,171] This alloy extends up into the QDs and generally becomes more In-rich with increased deposition (Fig. 10).[26,144,171] The concentration of In in both the wetting layer and the QDs increases with a decrease in the InAs growth rate.[171]

Some studies suggest adding an anneal step of 5 min at 580 °C before and/or after depositing the In$_x$Ga$_{1-x}$As.[164,168] The use of a surfactant, such as Te, can increase the critical wetting layer thickness up to 6 ML.[173] Houzay *et al.* were also able to obtain a critical
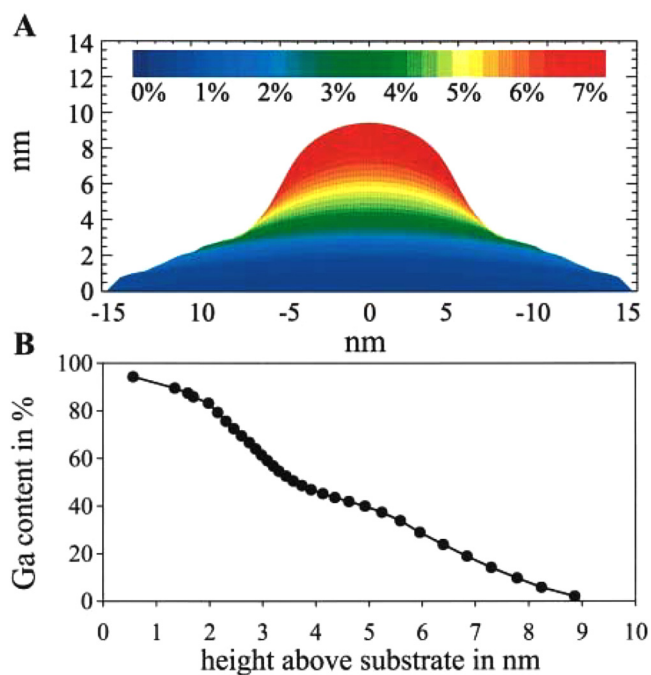

FIG. 10. Experimental results for the InAs/GaAs QD system. (a) Deviation of the lateral lattice parameter due to compositional variation in a QD compared to GaAs. (b) Ga-content of the In$_{1-x}$Ga$_x$As alloy in a QD as a function of vertical position. Reprinted with permission from Kegel *et al.*, Phys. Rev. Lett. **85**, 1694 (2000). Copyright 2000 American Physical Society.[167]

wetting layer thickness of 6 ML by depositing 0.5–1 ML InAs, pausing "several" minutes, and continuing the deposition at 0.05 ML/s.[166] The authors also show that it is possible to increase the wetting layer critical thickness to 3 ML by increasing the As overpressure during InAs growth.[166]

Ternary $In_xGa_{1-x}As$ QDs (i.e., $x < 1$) are often grown at slightly higher substrate temperatures of 505–530 °C.[26,170] Note that above ~530–540 °C, the sticking coefficient of indium falls rapidly to zero, placing an upper limit on the substrate temperature for QD growth.[175] For $x = 0.5$, the critical wetting layer thickness for $In_xGa_{1-x}As$ QD self-assembly increases to 4–5 ML.[26,170] An increase in the critical thickness is consistent both with the lower strain and the reduced availability of indium, meaning that it takes longer to reach the critical surface concentration for the transition to 3D growth (see Sec. IV C).[144]

When capping $In_xGa_{1-x}As$ QDs with GaAs to create the top barrier, it only takes ~5 nm for the streaky RHEED pattern to recover, indicating planar growth.[26] Typically, at least the first ~5–10 nm of the GaAs cap is grown at the QD growth temperature. This prevents indium-desorption when the sample is heated to the optimal substrate temperature for growth of the GaAs cap. We recommend growing a total GaAs cap thickness of at least 25 nm. However, if multiple layers of QDs are to be stacked in a given structure, tuning the spacer layer thickness may be required to prevent carrier tunneling or vertical alignment of QDs (if these effects are undesirable).[26,170,176] For further reading, the paper by Joyce and Vvedensky offers a comprehensive discussion of both GaAs homoepitaxy and InAs/GaAs heteroepitaxy.[171] The authors present information on surface reconstructions and demonstrate how substrate orientation impacts homo- and heteroepitaxy. In addition, the study by Jacobi provides a thorough discussion of InAs/GaAs QD facets and QD sizes.[174]

C. GaSb on GaAs(001)

GaSb QDs embedded within a GaAs matrix experience 7.8% lattice mismatch and exhibit a type-II band alignment offering hole confinement (Fig. 9).[36,119,168,172,177,178] QDs with type-II band alignments may be preferable for applications where low carrier recombination rates/long radiative lifetimes are required.[172,177,178] What is more, unlike type-I QDs, the emission energy from type-II QDs is tunable, blue-shifting as the cube root of the laser excitation density.[179,180]

We summarize our recommendations for growing GaAs(001) homoepitaxial buffers in Sec. V B. Once the GaAs buffer layer is complete, the substrate is cooled to 450–530 °C (we recommend 450–490 °C) while closing off the As flux (or dramatically reducing it).[36,119,172,177] We recommend exposing the GaAs buffer to a beam equivalent pressure (BEP) Sb_2 flux of ~1×10^7 Torr for 60 s prior to opening the Ga shutter.[119]

To grow the QDs, deposit 1.4–5 ML GaSb at a rate of 0.2–0.73 ML/s, with a V/III flux ratio of 1–2.[36,119,168,172,177] Once the critical wetting layer thickness of ~1.2 ML is reached,[150] the RHEED pattern transforms from streaky to spotty, indicating a transition to 3D self-assembly.[168,172] The result is defect-free GaSb (001) QDs.

Sun *et al.* show that to maintain GaSb QD quality, care during growth of the top barrier, or cap, is critical. After QD growth, increasing the substrate temperature above 500 °C results in "an immediate disappearance" of the spotty RHEED pattern.[172] The authors show that for GaSb QDs grown above 460 °C, the spotty RHEED pattern is maintained only if the substrate temperature is reduced to 460 °C under an Sb flux.[172] Once at 460 °C, the Sb valve can be closed, and the As valve opened.

Growth of a 50–100 nm GaAs cap can then take place.[172] It is common to deposit the first 10–15 nm GaAs at the GaSb QD growth temperature, before interrupting the growth and finishing the cap at standard GaAs growth temperatures close to 600 °C.[36,119,172,177]

For a droplet epitaxy method for growing GaSb/GaAs(001) QDs by MBE, see Liang *et al.*[119]

D. InAs on In$_{0.52}$Al$_{0.48}$As, In$_{0.53}$Ga$_{0.47}$As, or InP(001)

The compressive lattice mismatch of 3.2% between InAs and InP(001) (and its lattice-matched alloys $In_xAl_{1-x}As$ and $In_xGa_{1-x}As$) is considerably lower than the 7.2% mismatch InAs experiences on GaAs(001) (see Fig. 7). Because compressive strain serves to increase the semiconductor bandgap energy (Fig. 8), the lower strain in InAs/InP-based QDs means that their light emission/absorption is significantly red-shifted compared with similar QDs grown on GaAs. This red-shift means that InAs/InP-based QDs allow us to access the telecom-relevant "O" and "C" bands, centered at wavelengths of 1.3 μm and 1.55 μm, respectively.[181–185] These wavelengths correspond to minima in the absorption spectrum of standard silica optical fibers, where light transmission is more efficient. As a result, considerable research efforts have gone into obtaining room-temperature light emission from InAs QDs in these materials systems.[149,181–187]

An unusual feature of InAs self-assembly in these InP-based systems is the ability to synthesize either discrete QDs or elongated quantum wires (QWrs) depending on the MBE conditions, specific choice of buffer materials, or substrate offcut.[149,184,186–190] The InAs QWrs tend to line up parallel to the $[\bar{1}10]$ direction due to the anisotropic relaxation of strain (Fig. 11).[188,191] García *et al.* show that the group V stabilized (2 × 4) surface reconstruction gives rise to QWr formation in heteroepitaxial systems involving different group V elements.[191] Similar QWr formation effects have been reported in other mixed-group V systems, including InAs/AlAsSb (001).[180,192] In all cases, the QWrs form parallel to the dimer rows of the (2 × 4) reconstruction, which are aligned along $[\bar{1}10]$.[191]

Differences in QWr (or QD) morphology and light emission characteristics are observed when InAs is deposited on InP, $In_xAl_{1-x}As$, or $In_xGa_{1-x}As$.[149,181–187,193]

To grow self-assembled InAs QWr's or QDs, the InP(001) substrate oxide is desorbed at 500 °C for 10 min.[194] Regardless of the buffer material used, a 200–400 nm smoothing layer suffices for QD growth.[182–187,193]

For an InP buffer, we recommend growing at 1 μm/h and 400 °C under a P_2/In flux ratio of 20.[182,183,185–187,193] For $In_{0.53}Ga_{0.47}As$ or $In_{0.52}Al_{0.48}As$ buffers, a growth temperature of 460–525 °C is more common.[149,183,184,187] We recommend annealing the buffer at its growth temperature for 10 min under either an As or P flux depending on the buffer's group V element.[183,184]
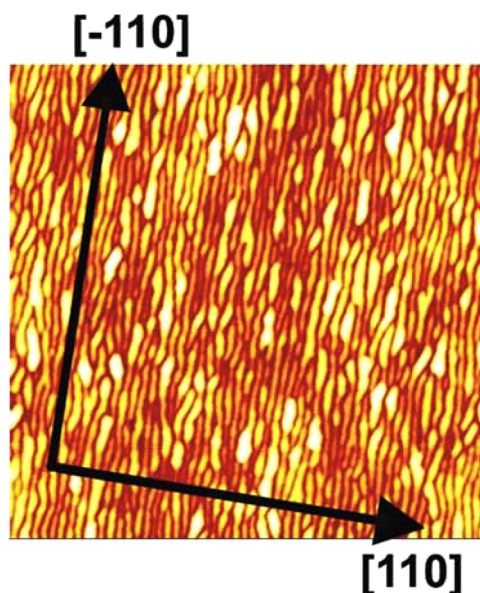
FIG. 11. $1 \times 1 \mu m^2$ AFM image of self-assembled InAs/InAlAs QWrs, showing their alignment parallel to $[\overline{1}10]$. Reprinted with permission from Simmonds et al., J. Vac. Sci. Technol. B **25**, 1044–1048 (2007). Copyright 2007 American Vacuum Society.[149]
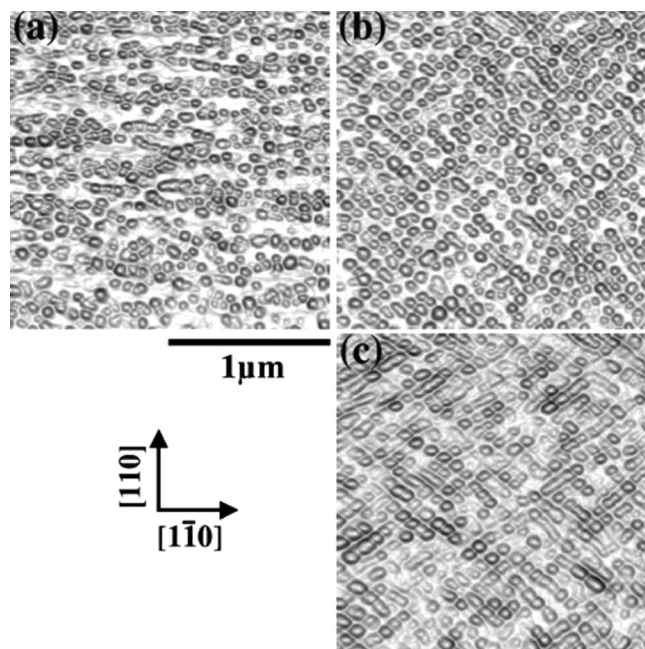

FIG. 12. AFM images of InP QDs grown on InGaP (a) lattice-matched to on-axis GaAs(001), (b) 0.60% lattice-mismatched to on-axis GaAs(001), and (c) 0.60% lattice-mismatched to GaAs(001) miscut by 2° toward ⟨111⟩A. Darker regions correspond to steeper facets. Reprinted with permission from Bortoleto et al., Appl. Phys. Lett. **82**, 3523–3525 (2003). Copyright 2003 AIP Publishing LLC.[197]

The InAs QD growth temperature is typically 400–495 °C on InP[184–186,193] and 460–525 °C on $In_{0.52}Al_{0.48}As$ or $In_{0.53}Ga_{0.47}As$.[149,183,184,187] Typical InAs growth rates are 0.1–0.5 ML/s under an As-rich overpressure where the V/III ratio is 30–35.[149,183–187,193] The critical thickness for the SK growth mode transition is ∼2.5 ML,[149,183–187] which is a result of the lower strain in this system compared to InAs/GaAs QDs (see Sec. IV C).

To tune QD size and areal density, some authors recommend annealing the self-assembled InAs after deposition for 30–120 s under the same substrate temperature and As flux.[183–187,193]

If growing more than one layer of self-assembled InAs, we recommend using 25–50 nm spacer layers grown under the same conditions as the bottom barrier.[181,187] Depending on requirements, a surface capping layer of 50–300 nm is sufficient to form a top potential barrier.[183–187]

E. InP on $In_xGa_{1−x}P$/GaAs(001)

InP QDs on $In_xGa_{1−x}P$/GaAs(001), with a maximum lattice mismatch of 7.2%, present an interesting opportunity to achieve highly organized, 2D arrays of QDs without substrate pre-patterning.[195–198] For $x = 0.51$, $In_xGa_{1−x}P$ is lattice-matched to GaAs, resulting in a 3.7% compressive lattice mismatch in the InP QDs. InP deposited onto lattice-matched $In_xGa_{1−x}P$/GaAs(001) can self-assemble into quantum rings.[199] Slightly straining the $In_xGa_{1−x}P$ with respect to the GaAs substrate can produce QDs with spatial alignment along the [100] and [010] directions (Fig. 12).[196,197] Many studies of this material system investigate the effect of the buffer composition on SK growth, QD elongation, and

QD shape.[195–198,200] There is evidence that the 2D wetting layer in this system is unstable. Corrosion of the wetting layer likely increases QD size.[197]

The initial steps for QD growth in this system involve the native oxide removal and the initial buffer growth of GaAs(001), which is described in Sec. V B. Typically, a 200–300 nm GaAs buffer is grown to smooth the surface, followed by the $In_xGa_{1−x}P$ bottom barrier.[25,195–200] 150–500 nm $In_xGa_{1−x}P$ is deposited at 0.5–1.0 ML/s, at a substrate temperature of 415–550 °C, under a P_2/III flux ratio of 10–32.[25,195–198,200] Smooth $In_xGa_{1−x}P$ buffers exhibit a streaky (2 × 1) RHEED pattern.[196–198]

Once the $In_xGa_{1−x}P$ growth is complete, the substrate temperature is adjusted for growth of the InP QDs, typically 410–540 °C.[25,195–198,200] InP QDs are deposited at 0.16–1.6 ML/s, usually at the lower end of that range.[195–200] The critical wetting layer thickness of the QDs is 1.5–3 ML, depending on the $In_xGa_{1−x}P$ buffer composition, and hence the amount of compressive strain in the InP. The 2D-to-3D SK transition is identifiable in RHEED from the telltale change from a streaky to spotty pattern.[195,198,200] The QDs are then capped with 10–100 nm of $In_xGa_{1−x}P$ to form the top barrier. Usually, the same MBE conditions are used in the top barrier as for the bottom barrier, although some groups suggest using migration-enhanced epitaxy for the first 10 nm of the $In_xGa_{1−x}P$ cap.[199]

F. $In_xGa_{1-x}As$ and $In_xGa_{1-x}P$ on GaP(001)

The growth of self-assembled QDs on GaP is of particular relevance to the integration of III–V semiconductors with Si. The ability to grow light emitters on a CMOS-silicon platform would have far-reaching technological implications. GaP is almost lattice-matched to Si and so is the natural substrate choice for developing suitable III–V semiconductor QDs such as $In_xGa_{1-x}As$ and $In_xGa_{1-x}P$.[38,44,201,202]

Although researchers struggled for many years to develop anti-phase domain-free GaP on Si, recent advances have minimized this deleterious effect.[201,202] In fact, high-quality GaP/Si substrates are now commercially available.[201,202]

Here, we provide recommendations for $In_xGa_{1-x}As$ and $In_xGa_{1-x}P$ QDs grown on GaP(001) nominally on-axis substrates.[38,39,44] These two materials systems boast maximum lattice mismatches of 7.7% for InP/GaP and 11.1% for InAs/GaP.[38,40,44] Both QD systems can emit light in the visible spectrum, in the range of 1.8–2.1 eV at $\sim$80 K.[39,40,44] The lower bandgaps of $In_xGa_{1-x}As$ compared with $In_xGa_{1-x}P$ mean that InGaAs QDs embedded within GaP will have stronger carrier confinement, an advantage for reliable operation at room temperature.[44] In addition, for $x < 0.3$, $In_xGa_{1-x}P$ is an indirect bandgap semiconductor rendering it incapable of light emission for these compositions (see Fig. 7).[39]

As for the previous examples of QDs made from ternary alloys, lattice mismatch in the $In_xGa_{1-x}(As,P)/GaP$ systems is tunable by controlling the composition. For example, $In_xGa_{1-x}As/GaP$ QDs with $0.07 \leq x \leq 0.5$ correspond to lattice mismatch in the range of 4%-7%. Since we can use compressive strain to widen the bandgap (Fig. 8), composition enables precise tuning of QD emission wavelength.[44]

For GaP(001) substrates, native oxide desorption occurs at 650 °C.[38,44] The GaP(001) substrate reveals a streaky, (2×4) RHEED pattern (Fig. 13).[38,40,44] To grow smooth GaP buffers, the substrate temperature is reduced to 560–620 °C.[38–40,44] The P_2/Ga flux ratio is $\sim$10,[44] and the growth rate is 0.4–0.7 ML/s.[39,44] We recommend a buffer thickness of at least 150–250 nm.[38,40,44]

To grow the $In_xGa_{1-x}(As,P)/GaP$ QDs, one cools the substrate to 490–510 °C, and either As_2 or P_2 is used for the QD deposition,[38,40,44,202] at a V/III flux ratio of $\sim$40.[44] QD growth rates of 0.013–0.2 ML/s are typical.[38,44]

For $In_{0.5}Ga_{0.5}As$ self-assembly via the SK growth mode, the critical wetting layer thickness is 1.9 ML.[44] For InAs/GaP QDs, however, there is evidence that the very high compressive strain leads to a VW growth mode.[38] For InP on GaP, the critical wetting layer thickness is 1.8–2.9 ML.[38,40] In all cases, the onset of 3D growth is accompanied by the transition from a streaky to a spotty RHEED pattern (Fig. 13).[38,40,44] The GaP cap should be grown under the buffer growth conditions.[38]

G. (Al)GaN on AlN

The InN, GaN, and AlN semiconductor family offers a wide range of bandgaps and lattice constants (Fig. 7), allowing researchers to engineer devices that can emit light from the visible to the ultraviolet parts of the spectrum. In the III-As materials system, the compounds GaAs and AlAs have almost identical lattice constants
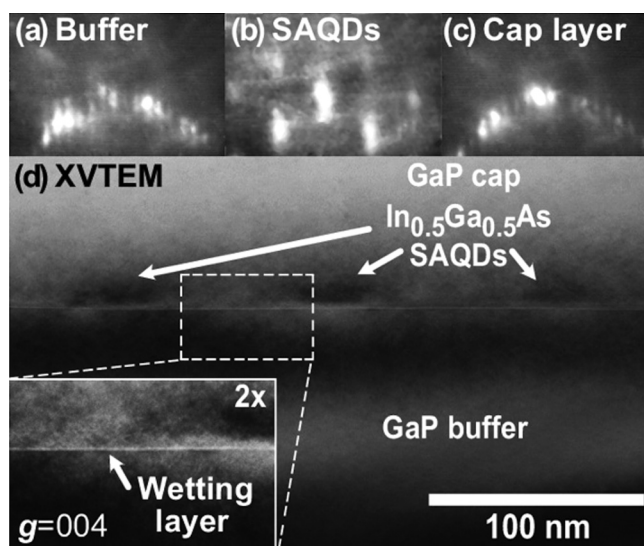

FIG. 13. (a)–(c) RHEED images showing the (2×4) pattern (a) before, (b) immediately after growth of 1.9 ML $In_{0.5}Ga_{0.5}As$ self-assembled QDs (SAQDs), and (c) after capping the QDs with GaP. (d) shows a cross-sectional TEM image of InGaAs SAQDs with an inset confirming the presence of a wetting layer and hence SK growth. Reprinted with permission from Song *et al.*, Appl. Phys. Lett. **97**, 223110 (2010). Copyright 2010 AIP Publishing LLC.[44]

ruling out strain-driven GaAs QD self-assembly. In contrast, there is a 2.5% lattice mismatch between GaN and AlN, which is *just* sufficient to enable the self-assembly of compressively strained GaN QDs on AlN via the SK growth mode.

For many years, the lack of free-standing III–N substrates meant that the majority of nitride growth was carried out on sapphire (α-Al_xO_3), 6H-SiC(0001), and 3C-SiC(001).[45] Researchers have used SiC substrates to integrate III–N LED technology with current Si electronics.[45,46] Growth on 3C-SiC(001) permits the growth of zinc-blende GaN.[47]

Damilano *et al.* showed the growth of GaN QDs on Si(111) substrates.[203] The lack of a native substrate meant that III–N samples suffered from very high threading dislocation densities. Thick buffer layers were hence needed to achieve high-quality epitaxy without effects from the substrate.[45,204] Low-defect, free-standing, and template III–N substrates are now commercially available, however, which has allowed researchers to achieve significantly improved epitaxial quality.[204]

Depending on the substrate material and the nitrogen source being used (e.g., N plasma or NH_3 gas), certain cleaning, annealing, and nitridating steps will be required.[45,47] For example, in the case of an rf source, some groups expose sapphire substrates to the N plasma for 1 h at 870 °C to form a reactive $Al_xO_{1-x}N$ surface layer.[45] Plasma powers are typically around 300 W, with N flow rates of $\sim$1 sccm.[133] After this process, a 10–30 nm layer of AlN is grown at 650–730 °C, with an optional step of growing 2 μm of GaN. Following this step, a further 0.2–1.5 μm of AlN can be grown at 500–550 °C.[45] The GaN QDs can then be grown on top of this buffer.

Depositing the GaN at substrate temperatures below 620 °C results in the smooth, FM growth mode; it is only at higher temperatures that we see the transition to self-assembly of GaN QDs via the SK growth mode.[45] GaN/AlN QDs are, therefore, grown at substrate temperatures of 680–730 °C by depositing 2–4 ML of GaN.[45] Gačević et al. used a growth rate of 0.3 ML/s at a substrate temperature of 720 °C.[205] The 2.5% lattice mismatch between GaN and AlN means that the critical thickness of the 2D wetting layer is 2–2.5 ML.[45,133]

Schupp et al. grew GaN on a 3C-SiC(001) substrate by growing a 30 nm AlN buffer at 730 °C.[206] Depositing GaN onto the AlN, they report a critical thickness for the 2D-to-3D growth transition of 2 ML.[206] The resulting QDs present an areal density of 5×10^{11} cm^{-2}, with average heights and diameters of 3 nm and 15 nm, respectively.[206]

As et al. reported the self-assembly of GaN QDs on a 3C-SiC (001) substrate that had first been chemically etched and then annealed for 10 h at 500 °C.[207] They then deposited the GaN at 720 °C directly on the SiC substrate.[207] More recently, Bürger et al. used a Si substrate, on which they grew a 10 μm 3C-SiC(001) buffer layer.[204] Using a N plasma source, the team used Al flashes to clean the surface at 910 °C before cooling it to 760 °C to grow 30 nm of AlN.[204] Upon completion of the AlN barrier layer, they deposited GaN in different amounts; using PL spectroscopy, they pinpointed the critical thickness for the SK transition at 1.95 ML.[204] They also showed an increase in the average areal density of these QDs from 10^{10} cm^{-2} at 2 ML of deposition to 10^{11} cm^{-2} at 3 ML.[204]

We recommend using these growth conditions established by Bürger et al. as they have also been used by Blumenthal et al. for a study of the optical characteristics of these GaN QDs.[208]

There is currently considerable research interest in creating mercury-free light emitters operating at ultraviolet (UV) wavelengths. Recent studies propose to create UV-emitting LEDs based on wide-bandgap $Al_yGa_{1-y}N$ QDs grown on $Al_xGa_{1-x}N$ at various concentrations.[209,210] Brault et al. grew a low-temperature GaN buffer on a sapphire (0001) substrate followed by 100–150 nm of AlN grown at 950 °C. They then grew 0.8–1 μm of Si-doped $Al_{0.6}Ga_{0.4}N$ at 850–870 °C.[209,210] This layer serves as the bottom barrier for QD nucleation. The researchers decreased the substrate temperature to 720–730 °C and deposited 8–10 ML $Al_yGa_{1-y}N$ with concentrations of $y = 0.1 - 0.4$. The V/III flux ratio was 0.7 with a growth rate of 0.1–0.4 ML/s. The critical thickness observed for the SK formation of QDs is between 3 and 4 ML.[209,210] The QDs were then annealed in vacuum for 6 min and then heated to 820 °C to improve QD uniformity.[209] A 30 nm top layer of $Al_{0.6}Ga_{0.4}N$ was used to cap the sample. The authors use NH$_3$ for growing the GaN and AlGaN layers but switch to a N$_2$ plasma source for the QD layers.[209,210] The resulting QDs have densities of $1.5–5.4 \times 10^{11}$ cm^{-2}, heights between 1.5 and 3 nm, and diameters of 5–20 nm.[209,210] Other groups have grown UV LED structures under similar conditions but containing multiple layers of QDs.[211]

It is possible to tune GaN QD size, areal density, and morphology by growing them under either N-rich (N/III flux ratio >1) or Ga-rich growth (N/III flux ratio <1) conditions.[45,133,205,212–214] Under N-rich conditions, adatom mobility is reduced, leading to small GaN QDs with high areal density (typically

$10^{11}–10^{12}$ cm^{-2}).[45] Ga-rich conditions increase adatom mobility, resulting in larger GaN QDs whose areal density is 1–2 orders of magnitude lower.[205]

Ostwald ripening provides a reliable way to control the areal density (Fig. 14). At a sufficiently high substrate temperature, annealing the GaN QDs under a N plasma for ~50 s decreases the
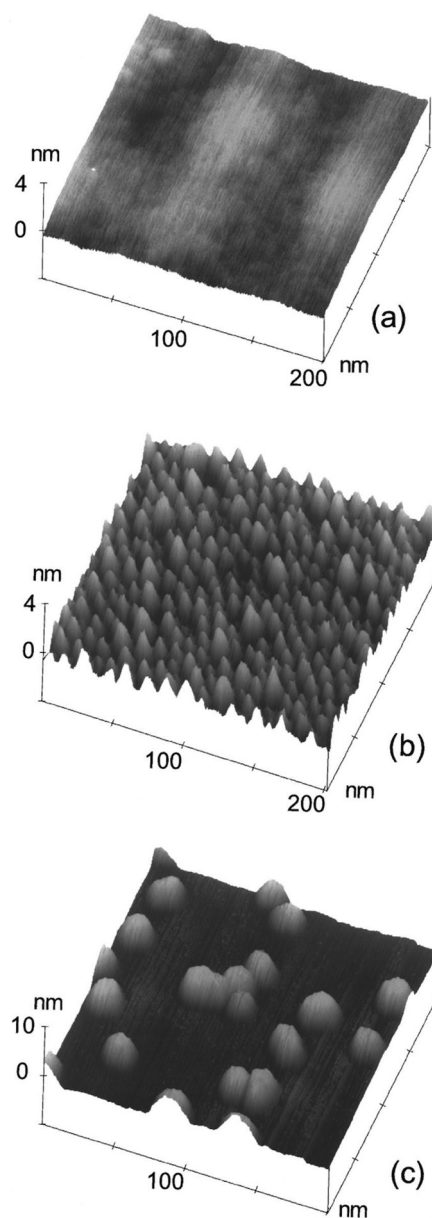

FIG. 14. AFM scans of (a) a smooth AlN surface, (b) GaN QDs cooled rapidly after growth, and (c) GaN QDs annealed for 50 s in N plasma after growth. Reprinted with permission from Daudin et al., Phys. Rev. B **56**, R7069 (1997). Copyright 1997 American Physical Society.[212]

areal density while increasing the average QD size.[45] Due to the nucleation of QDs on threading dislocations, bimodal distributions of QD size have been reported.[133] QD size uniformity was improved by growing multiple QD layers to form a superlattice.[133] When stacking multiple layers of GaN QDs, a vertical correlation between adjacent QD layers was observed for AlN spacers ≤8 nm thick.[45]

H. In$_x$Ga$_{1-x}$N on GaN

Similar to the GaN/AlN system, In$_x$Ga$_{1-x}$N on GaN offers the possibility of compressively strained QDs with high quantum efficiency for LED applications (Fig. 15).[45,47] Again, using sapphire as the example substrate, researchers begin by growing a 2 μm GaN buffer.[45] Adelmann et al. then deposited an In$_{0.35}$Ga$_{0.65}$N layer (lattice mismatch of 3.9%) at 580 °C and noted that the critical thickness for the 2D-to-3D SK transition occurred at 1.7 ML.[48] As the In$_{0.35}$Ga$_{0.65}$N deposition amount is raised to 5 ML, the resulting QDs have an areal density of 10^{11} cm^{-2}, with an average diameter and a height of 27 nm and 2.9 nm, respectively.[48] These QDs exhibit strong blue-violet PL, even at 300 K.[48]

Indeed, Damilano et al. show that the self-assembly of In$_x$Ga$_{1-x}$N/GaN QDs is possible with indium compositions as low as $x = 0.12$.[203] As the strain is reduced, the critical thickness for the SK growth mode transition increases accordingly (see Sec. IV C). For example, for In$_{0.15}$Ga$_{0.85}$N/GaN QDs grown at 530–570 °C, the critical thickness is 5 ML for $x = 0.15$, and the resulting QDs have an average areal density of 5×10^{11} cm^{-2}, with an average diameter and a height of 35 nm and 4 nm, respectively.[203]

Gačević et al. grew In$_{0.5}$Ga$_{0.5}$N/GaN QDs at substrate temperatures of 520–580 °C. After completing 12 ML deposition, the researchers annealed the sample for 1 min before cooling. The average QD areal density for this growth is 7×10^{10} cm^{-2}, with an average height and a diameter of 3 and 30 nm, respectively.[205]

Binary InN/GaN QDs ($x = 1$) self-assemble via the VW growth mode (i.e., no wetting layer) due to the 11% lattice mismatch (see Sec. IV B).[133] After the usual GaN buffer growth, the substrate was cooled to 425 °C, before depositing 9 ML of InN at a growth rate of 0.05 nm/s. The sample was then annealed under N for 5 min before cooling down.[133] The QD density for this sample was 2×10^9 cm^{-2}, with an average QD diameter and a height of 115 and 15 nm, respectively. The absence of a wetting layer indicates nucleation of InN QDs directly on the GaN threading dislocations.[133] The QDs have a wurtzite structure and are epitaxial to the GaN buffer layer.[133]

I. CdSe on ZnSe

Self-assembled QDs in the II–VI semiconductors combine all the advantages of QDs mentioned so far (bandgap tunability, enhanced quantum efficiency, limited post-growth processing) but with bandgap energies that correspond to the visible spectrum.[49,50] Similar to the In$_x$Ga$_{1-x}$As/GaAs system (see Sec. V B), the lattice mismatch values for the CdSe/ZnSe and CdTe/ZnTe systems are 6.3% and 5.8%, respectively.[50,215]

The offset in the bandgap between CdSe and ZnSe is comparable to that in archetypal InAs/GaAs QDs, enabling similarly strong quantum confinement of carriers. As a result of the
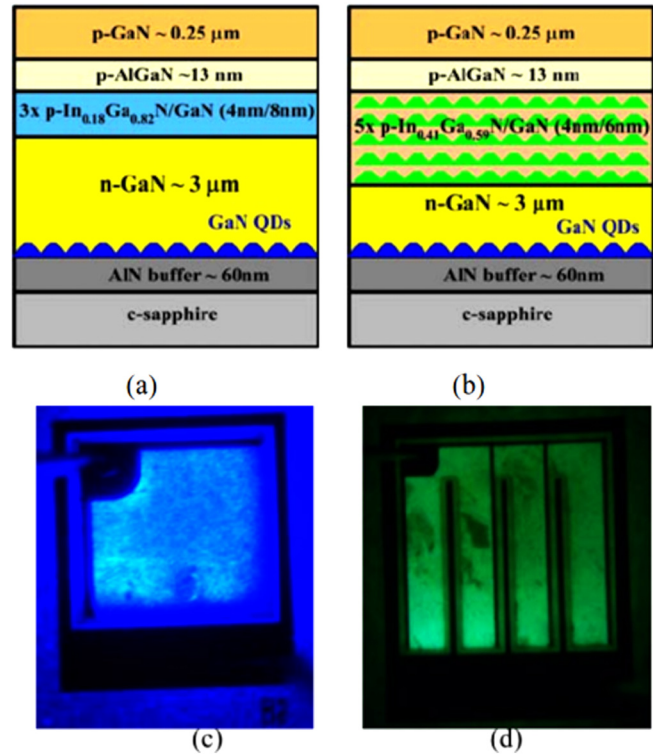

FIG. 15. (a) and (b) are schematics for the LEDs in (c) and (d), respectively. In (a) and (c), an InGaN/GaN QW is used to emit blue light, whereas in (b) and (d), InGaN/GaN QDs are used to produce green light. Reprinted with permission from Moustakas et al., Phys. Status Solidi A **205**, 2560–2565 (2008). Copyright 2008 Wiley-VCH Verlag GmbH & Co. KGaA.[133]

chemical species present in II–VI materials, we can study QD formation in these material systems to deconvolve the contributions to self-assembly from surface energy and strain.

The critical thickness for CdSe/ZnSe QDs is not well established. Indeed, several studies show that the SK growth mode transition has to be induced.[50,216,217]

Xin et al. synthesized CdSe QDs on ZnSe by first growing a 2 μm ZnSe buffer at 300 °C on a GaAs(001) substrate.[49] At this point, the RHEED showed a streaky (2 × 1) pattern. The team then increased the substrate temperature to 350 °C and deposited CdSe at a growth rate of 0.4 ML/s. The RHEED pattern became spotty, indicating a transformation from 2D to 3D growth.[49] They buried the CdSe QDs with a 50 nm of ZnSe.[49] The QD areal density in their samples was 2.5×10^9 cm^{-2}, with an average QD diameter of 40 ± 5 nm and a height of 10 ± 3 nm.

Robin et al. developed a method to induce the 2D to 3D transition in smooth, strained CdSe layers.[216] After the growth of 3 ML CdSe by atomic layer epitaxy, the sample is cooled below room temperature and an amorphous Se layer is deposited. The substrate temperature is then ramped up to 230 °C to desorb the amorphous Se and achieve a bright spotty RHEED pattern, consistent with 3D

self-assembly.[216] The critical thickness found by the researchers is 3 ML; depositions below that produce only undulations on the surface.[216]

CdSe QDs grown on $Zn_{1-x}Mn_xSe$ (with $x = 0.05$ and 0.10) have a higher areal density and a smaller average size than CdSe/ZnSe QDs due to the reduced compressive strain.[49] Merz et al. studied the same system as Xin et al., but with a slightly higher substrate temperature and a lower growth rate (370 °C and 0.025 ML/s, respectively). From RHEED, they show that QDs begin to appear after deposition of 3.0–3.5 ML of CdSe,[219] consistent with other groups who place it in the range of 2.5–3.0 ML.[220] These results rule out VW self-assembly.

Researchers capped some CdSe QDs with a 50 nm of ZnSe for PL while doing AFM on uncapped samples within 1 h of unloading to study their morphology.[219] The QDs are relatively circular in shape, with an areal density of 2×10^9 cm^{-2}. AFM scans performed at 48 h intervals show that surface CdSe QDs undergo Ostwald ripening at room temperature, a phenomenon not observed on III–V QD systems (see Fig. 16). As a consequence, areal density decreases, and the average QD size distribution broadens. The rate of change in the areal density with time shows that the ripening occurs through interface-transfer-mediated growth.[220] Extrapolation shows size uniformity at the moment of deposition. Daruka and Barabási refer to this transition from a wetting layer to
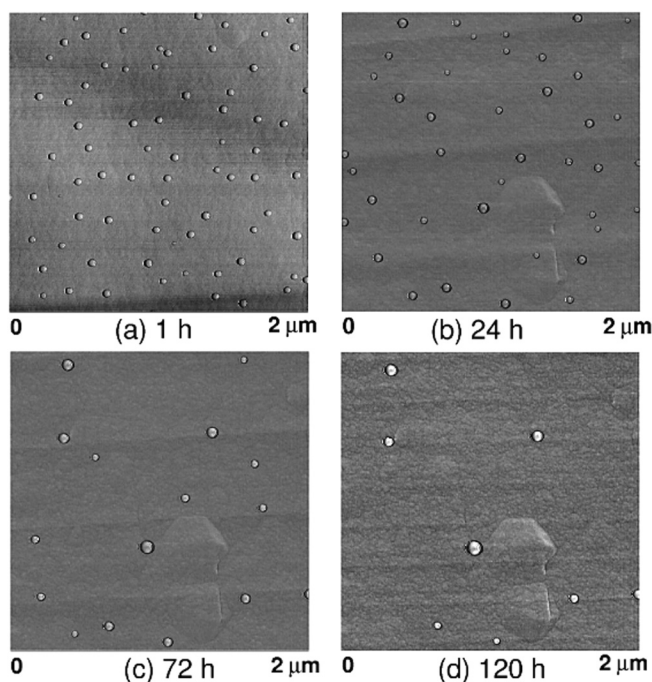

FIG. 16. Bright-field TEM images of the same region of a sample of CdSe/ZnSe QDs showing room-temperature ripening of the QDs (a) 1 h, (b) 24 h, (c) 72 h, and (d) 120 h after the sample was removed from the MBE chamber. Reprinted with permission from Lee et al., Phys. Rev. Lett. **81**, 3479 (1998). Copyright 1998 American Physical Society.[218]

islands that ripen as "Regime I."[221] Cooling the samples to 0 °C prevented this ripening effect.[219]

Rabe et al. grew 1 μm of ZnSe on GaAs(001) at 310 °C.[222] After growing the buffer, the sample is cooled down to 230 °C under Se-rich conditions. They then deposit a few monolayers of CdSe, which grows in a layer-by-layer mode. Then, while keeping the Se shutter open, they heat the substrate to 310 °C, at which point they observe a transition to 3D self-assembly in the RHEED pattern.[222] Immediately after the CdSe deposition, samples are capped with 85 nm of ZnSe. Sample analysis using PL showed researchers that the QDs form on top of a 2 ML wetting layer.[222]

Kratzert et al. studied the thermally activated transition of QDs more closely by growing a ZnSe buffer on GaAs(001) at 230 °C, depositing 3 ML of CdSe at the same temperature, and then heating the sample to 310 °C. Surface analysis with ultrahigh vacuum AFM showed reproducible and consistent QDs averaging 1.6 ± 0.3 nm in height and 10 nm in diameter.[223] Maćkowski et al. found that doping with Mn atoms affects the emission from these QDs by interacting with the magnetic ions provided as dopants.[224] Kurtz et al. showed that when using a CdS source for Cd during the growth of these QDs, the S can act as a surfactant.[225]

J. CdTe on ZnTe

CdTe/ZnTe QDs are an interesting system for the growth of diluted magnetic materials (DMS), with applications in quantum information technologies.[51] Controlling CdTe QD growth of CdTe QDs is critical to enable the subsequent incorporation of magnetic ions.[51]

Karczewski et al. began by growing a 4.5 μm CdTe buffer on GaAs(001) at 420 °C, followed by 100 nm of ZnTe.[52] They deposited 1.5, 2.0, and 2.5 ML CdTe to form thin, QD-like structures, with an average diameter of 3 nm and a density of 10^{12} cm^{-2}. Interestingly, they did not observe a 2D-to-3D transition in the RHEED pattern.[52] After QD growth, they annealed the sample for 20 s and then grew a 100 ML ZnTe top barrier. The authors argue that the PL characteristics of the CdTe QDs suggest enhanced quantum efficiency.[52]

Tinjod et al. demonstrate that both strain and surface energy are important factors in CdTe/ZnTe(001) QD formation.[215] They grew CdTe on ZnTe in a layer-by-layer mode at 280 °C. They then covered the samples with amorphous Te at room temperature, before heating the sample back up to 220 °C to desorb the Te, at which point the RHEED pattern is spotty when it reappears.[215] This thermal activation (TA) step promotes QD formation by changing the sample's surface energy and was later adopted by other researchers.[51,226,227] The ionic nature of a Te-rich II–VI surface increases the 2D surface energy, thus decreasing the cost for facet creation and favoring a 3D transition. Using this information, groups grew self-assembled CdTe QDs on a $Zn_{0.8}Mg_{0.2}Te$ alloy with a lower lattice mismatch of 5%.[215]

Wojnar et al. studied how to control the properties of CdTe/ZnTe QDs by in situ annealing of the QD ensemble before deposition of the cap layer. They showed that QDs and 0D quasi-islands form by potential fluctuations at the interfaces of the quasi-wetting layer.[226] They grew 1 μm of ZnTe, followed by 6 ML of CdTe to form the QDs, and then applied the TA step. The researchers

annealed the samples under a Te flux, before depositing a 100 nm ZnTe cap. Annealing below 380 °C results in Ostwald ripening of the QDs. Extended annealing at higher temperature causes the RHEED to revert to a streaky 2D pattern.[226]

Sorokin *et al.* demonstrated the growth of CdTe/Zn(Mg)(Se) Te QDs using the TA technique.[227] They grew 200 nm of InAs on InAs(001) at 295–300 °C to obtain a (2×4) surface reconstruction. They then deposited 5 ML of ZnTe, followed by 10 nm of $Zn_{0.9}Mg_{0.1}Te$, 20 nm of ZnTe, 3.0–5.5 ML of CdTe, and finally capped the sample with 20 nm of ZnTe. After depositing the CdTe, they carried out the TA step, followed by 30–40 min at 300 °C with and without a Te overpressure. From PL, the authors estimate a QD areal density of 10^{10} cm^{-2}.[227] The same team reported CdTe QDs in barriers of quasi-quaternary ZnMgSeTe in the form of short period superlattice (SL) ZnTe/MgTe/MgSe with 2 nm periods. The structures are composed of 5 ML ZnTe and a 150 nm short period ZnTe/MgTe/MgSe SL, followed by 3 ML CdTe QD layers separated by 3 ML ZnTe spacers, and a 45 nm top barrier consisting of another ZnTe/MgTe/MgSe SL.[228]

VI. TENSILE-STRAINED QUANTUM DOTS

Research interest in tensile-strained self-assembly has grown steadily since around 2005.[53,229–232] Tensile strain occurs when the lattice constant of the QD material is smaller than that of the surrounding matrix. The lattice constant of most semiconductors is inversely related to their bandgap (Fig. 7). Correspondingly, the QD and matrix materials must be selected carefully to achieve quantum confinement. However, this constraint imposed by the limited number of suitable QD-matrix band alignments is relaxed somewhat by the fact that tensile strain has the opposite effect to compressive strain and serves to reduce the bandgap energy [Fig. 8(c)]. Light emitted or absorbed by tensile-strained QDs is hence red-shifted, and as a result, they are optically active below the effective bandgap of the corresponding unstrained material.[56–58] In addition, tensile strain pushes the light-hole band above the heavy-hole band [Fig. 8(c)]. The possibility of QDs that naturally exhibit a light-hole exciton ground state is extremely attractive for quantum media conversion and other applications.[233,234]

To ensure defect-free self-assembly, researchers typically grow tensile-strained QDs on (110) and (111) substrates instead of (001).[55] The characteristics of these non-traditional surface orientations give tensile-strained QDs some unusual properties. For

example, under sufficient tensile strain, Ge on a (110) surface orientation should become a direct bandgap semiconductor useful for light-emitting infrared devices.[235–238] (111)-oriented QDs are widely expected to exhibit low fine-structure splitting.[38–40,44,66,235] As we discuss in Sec. II C, low fine-structure splitting is essential if a QD is to be used as a source of entangled photons for quantum information applications.

That being said, the growth of high-quality buffers on (110) and (111) surfaces is notoriously difficult. Researchers have invested considerable effort to identify MBE conditions that produce smooth buffer surfaces required for subsequent growth of tensile-strained QDs.[55–57,59,139,239–241] As a direct result of these efforts, research into tensile-strained QDs is growing quickly. The relative youth of this field means that there is a great deal still to discover.

A. GaAs on InAlAs(110) and (111)A

As noted above, self-assembled GaAs QDs with a (111)A orientation exhibit a low fine-structure splitting, suitable for entangled photon emission via the biexciton–exciton cascade.[58] Because of the low bandgap, tensile strain, and type-I band alignment in this system, these QDs on both (111) and (110) substrate orientations could also be used for near-IR optoelectronics.[56,58–60,242] Additionally, the GaAs/InAlAs(111)A QD system presents an unusual opportunity to tune the wetting layer thickness beyond the critical thickness.[58,60]

GaAs(111)A QDs are grown on nominally on-axis InP(111)A substrates, where the tensile lattice mismatch is 3.7% (Fig. 17).[58–60,242] The native oxide is removed by heating the InP substrate to 510 °C for 15 min under an As$_4$ flux.[139] The substrate temperature is then slightly adjusted to 495–510 °C for the buffer growth.[58–60,139,242] A 50 nm $In_{0.53}Ga_{0.47}As$ (hereafter simply InGaAs) buffer is deposited, which promotes surface smoothing.[241] This is followed by 200 nm $In_{0.52}Al_{0.48}As$ (hereafter simply InAlAs) for the bottom barrier. Both the InGaAs and InAlAs are grown at a rate of ~170 nm/h with a high V/III flux ratio of ~160.[58–60,139,242]

The substrate is then brought to the desired QD growth temperature, typically between 460 and 540 °C.[58–60,242] The As valve is partially closed to reduce the V/III flux ratio to ~75, and GaAs is deposited at a rate of 0.025–0.125 ML/s.[58–60,242] The critical thickness for the 2D-to-3D SK transition is 2.5 ML.[59,60] This critical

(a) 1 ML GaAs   (b) 2.5 ML GaAs   (c) 4.5 ML GaAs

3 nm

400 nm

TSQD Volume: 417 nm³
Density: 6.8 × 10⁷ cm⁻²

TSQD Volume: 1102 nm³
Density: 4.4 × 10⁸ cm⁻²

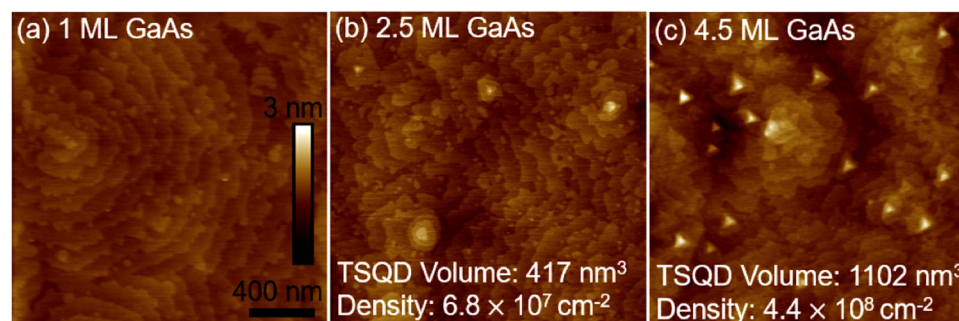**FIG. 17.** $2 \times 2 \, \mu m^2$ AFM images revealing the evolution of GaAs(111)A TSQD morphology with increasing deposition: (a) 1 ML GaAs showing the smooth 2D wetting layer, (b) 2.5 ML GaAs showing the onset of 3D TSQD self-assembly, and (c) 4.5 ML GaAs showing mature TSQD formation. Reprinted from Schuck *et al.*, Sci. Rep. **9**, 1–10 (2019). Copyright 2019 Springer Nature.[60]

thickness is determined by AFM since the streaky (2 × 2) RHEED pattern does not change during GaAs deposition.[59,60] We believe that the combination of a low areal density (10^8–10^9 cm^{-2}) and a small height (typically <2 nm) of the QDs means that the interaction between the electron beam and the GaAs in the QDs is insufficient to generate a spotty pattern. The streaky RHEED pattern of the smooth tensile-strained GaAs wetting layer between the QDs, therefore, dominates.[59,60]

The QDs are covered by 10 nm of InAlAs, grown at the QD growth temperature.[58–60,242] The growth is then interrupted and the substrate is heated back to 495–510 °C to grow the rest of the InAlAs top barrier (another 30–40 nm).[58–60,242] The sample is typically completed by growing another layer of GaAs QDs on the surface for morphology studies or with a 5–10 nm InGaAs cap to prevent oxidation of the InAlAs top barrier.[58–60,242]

For tensile-strained GaAs(110) QDs, a nominally on-axis InP (110) substrate is degassed at 500 °C for 30 min under an As$_4$ overpressure.[56] The substrate temperature is decreased to 300 °C, and 200 nm InAlAs is deposited at 0.5 μm/h, with a V/III flux ratio of 80.[56] The substrate is then annealed at 500 °C for 15 min.[56] Once the buffer is annealed, GaAs is deposited at 0.1 ML/s, with a V/III flux ratio of 65.[56] The critical thickness for the 2D-to-3D transition is 1.6 ML, which again is established with AFM since the streaky (1 × 1) RHEED pattern of the unreconstructed (110) surface does not change during GaAs deposition [see the discussion of GaAs (111)A QDs above].[56] To cap the QDs, the substrate is cooled back to 300 °C to grow the top InAlAs barrier under an As$_4$ flux.[56] We recommend a cap thickness of >50 nm, and if not depositing surface QDs, the growth of a thin, 5–10 nm InGaAs cap is to prevent oxidation of the InAlAs top barrier.[56]

B. Ge on InAlAs(111)A

Recently, researchers have developed a method of growing tensile-strained Ge QDs within an In$_{0.52}$Al$_{0.48}$As(111)A matrix lattice-matched to InP (Fig. 18).[139] For a (111) substrate orientation, the 3.7% tensile lattice mismatch between Ge and InP is expected to reduce Ge's bandgap to zero, transforming this well-known semiconductor into a semimetal.[243] Semimetallic Ge(111) QDs could be useful for high-efficiency solar cell tunnel junctions, thermoelectric materials, or even as a novel route to topological insulators.[244–247] Unusually, researchers are able to select either SK or VW for tensile-strained Ge QD self-assembly, simply by controlling the substrate temperature.[139]

After removing the InP(111)A oxide, an InGaAs smoothing layer is grown, followed by an InAlAs bottom barrier (see Sec. VI A).[139] The substrate temperature is then adjusted to 435–560 °C for Ge QD growth, before closing the As valve and shutter.[139] After waiting 60 s for the As overpressure to reduce, they deposited 0.2–1.2 bilayers (BL) of Ge at 0.010–0.025 BL/s.[139] Upon deposition, the RHEED pattern swiftly develops from streaky (2 × 2) to spotty, indicative of 3D self-assembly.[139]

Ge QDs grown at substrate temperatures below 510 °C self-assemble via the SK growth mode. An initial 2D wetting layer forms, with a critical thickness for the 2D to 3D transition of 0.6 BL at 435 °C. The critical thickness decreases as the substrate temperature is raised, until at ≥510 °C, the Ge QDs self-assemble
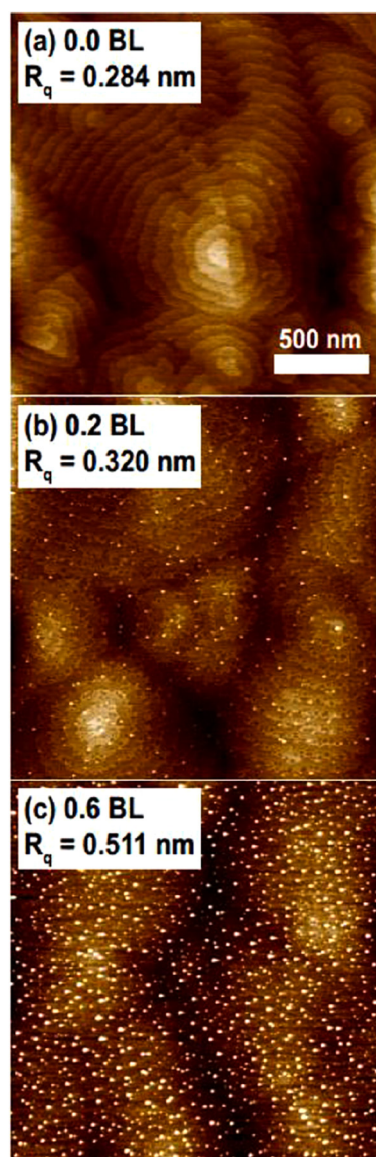
FIG. 18. $2 \times 2\,\mu m^2$ AFM images showing the evolution of Ge(111)A TSQD morphology with increasing deposition: (a) 0 BL Ge, i.e., the bare InAlAs(111)A surface, (b) 0.2 BL Ge, and (c) 0.6 BL Ge. The z-scalebar is 2 nm for all images. Reprinted with permission from Sautter et al., J. Cryst. Growth **533**, 125468 (2020). Copyright 2020 Elsevier.[139]

via the VW growth mode (i.e., the critical thickness of 0 BL).[139] After Ge QD growth, the substrate is heated to ~500 °C to grow the top InAlAs barrier, followed by a 5 nm InGaAs cap (if not growing a surface layer of QDs for AFM).[139] A follow-up study of Ge QD self-assembly on InAlAs(110) is under way, for which the InAlAs/InGaAs buffer conditions will be similar to those discussed in Sec. VI A.

C. Additional tensile-strained self-assembly systems

Although this section discusses self-assembly, not all of the resulting 3D nanostructures are optically active. Some are composed of indirect bandgap semiconductors. For others, the nanostructure bandgap is larger than that of the surrounding matrix, preventing carrier confinement and hence light emission. As a result, they cannot be considered true QDs; therefore, we instead describe them as "nanostructures."

We include this section for historical and practical reasons since the studies described below typically discuss not only how to grow the tensile-strained nanostructures but also the smooth buffer surfaces beneath. These buffers include materials such as Ge(111), GaAs(110), and GaAs(111). Interest in semiconductor systems with non-(001) orientations is growing,[241] and these materials could represent useful starting points from which to investigate new tensile-strained QD systems.

Si on Ge(111) was one of the earliest tensile-strained systems investigated. Researchers demonstrated the self-assembly of tensile-strained defect-free Si nanostructures.[137] They start with 40 nm Ge at 380 °C, followed by 40 nm $Ge_{0.85}Si_{0.15}$ at 500 °C. The substrate is heated to 450–650 °C for Si deposition. After deposition, the substrate is immediately cooled. The resulting defect-free Si(111) nanostructures form via the VW growth mode, with tunable size and areal density.

Building on that early report, Simmonds and Lee moved to III–V semiconductors to carry out a comprehensive investigation into the relationship between surface orientation and a sign of strain sign (Fig. 19).[53–55] They showed that both factors must be considered to predict whether strain relief is elastic (i.e., via 3D nanostructure formation) or plastic (i.e., via dislocation nucleation and glide).[53–55] The result of their study was to predict that defect-free, tensile-strained nanostructures would self-assemble, as long as they were grown on either (110) or (111)-oriented substrates.[53–55]

To test this prediction, they focused on the growth of GaP on GaAs, which experiences a tensile lattice mismatch of 3.7%.[53–55] They showed that when GaP is grown on GaAs(001), the tensile strain is relieved plastically and self-assembly does not occur. However, when GaP is grown on GaAs(110) or (111) surfaces, the tensile strain is relieved elastically, and defect-free 3D GaP nanostructures self-assemble via the VW growth mode.[53–55] Although optically inactive due to GaP's indirect bandgap, the spontaneous formation of these tensile-strained nanostructures confirmed the model's prediction. This result provides a deeper understanding of QD self-assembly: namely, that we can grow QDs with either compressive *or* tensile strain, provided we select the correct substrate orientation.

For GaP/GaAs(110) nanostructures, the GaAs(110) substrate is first degassed at 610 °C for 20 min under an As_4 overpressure.[53,55] For the GaAs(110) homoepitaxial buffer, the substrate temperature is reduced to 540 °C. The buffer is typically 60 nm thick and is grown at 0.45 µm/h with a relatively high V/III flux ratio of 75.[53,55] The buffer is then annealed for 15 min at 600 °C to promote surface smoothing.[53,55]

For GaP/GaAs(111)A nanostructures, the GaAs(111)A substrate is first degassed at 630 °C for 30 min under an As_4 overpressure, and then the substrate temperature is reduced to 540–600 °C
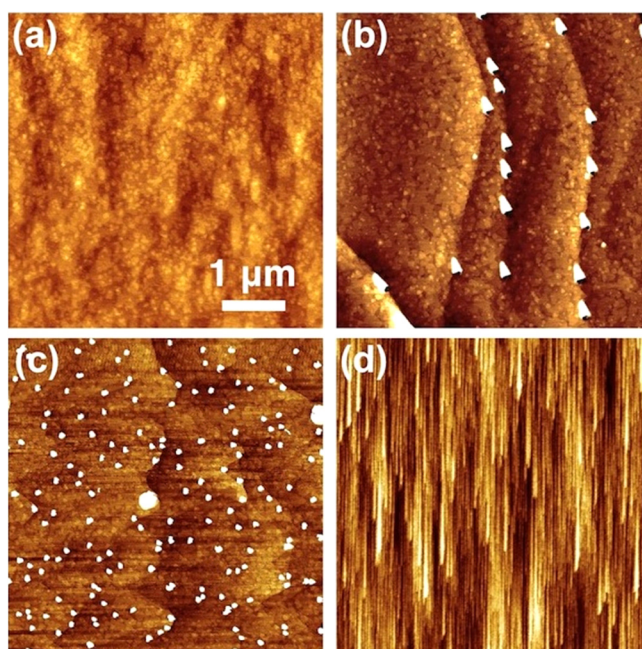

FIG. 19. $5 \times 5\,\mu m^2$ AFM images showing the results of growing (a) a 4.5 ML GaP film on GaAs(001) (3 nm z-scale), (b) 4.2 ML GaP QDs on GaAs(110) (3 nm z-scale), (c) 1.7 ML GaP QDs on GaAs(111)A (5 nm z-scale), and (d) 3.9 ML GaP QWrs on GaAs(111)B with a 2° miscut (5 nm z-scale). Reprinted with permission from Simmonds and Lee, J. Appl. Phys. **112**, 054313 (2012). Copyright 2012 AIP Publishing LLC.[55]

for homoepitaxial buffer growth.[54,55] The GaAs(111)A buffer is grown under a V/III flux ratio of 70 and a growth rate of 0.45 µm/h.[54,55] After depositing ∼60 nm GaAs(111)A, the substrate is annealed at 640 °C under an As_4 overpressure for 15 min to promote surface smoothing.[54,55]

Both surface orientations use similar GaP growth conditions. After annealing the buffer surface, the substrate temperature is reduced to grow the GaP nanostructures, typically between 460 and 580 °C, under an As_4 overpressure.[53–55] Once at the desired QD growth temperature, the As valve is closed for 20 s to reduce anion mixing, before opening the Ga and P_2 sources to deposit the GaP.[53–55] 0.2–6.4 ML of GaP is deposited at 0.014–0.142 ML/s, with a V/III flux ratio of 10–12.[53–55] Since these nanostructures were mainly used for surface studies, the substrate was then immediately cooled under a P_2 overpressure.[53–55]

A small number of other studies exist in which researchers have explored the use of tensile strain to drive nanostructure self-assembly by MBE. Toropov *et al.* and Meltser *et al.* demonstrate the growth of GaAs/GaSbAs(001) QWs with a 7.5% tensile lattice mismatch. QDs form spontaneously within these QWs as a result of compositional inhomogeneities.[229,230] Taliercio *et al.* demonstrated $In_xGa_{1-x}As/GaSb(001)$ quantum wells with some signs of QD formation.[231] Lenz *et al.* studied GaAs/GaSb(001) tensile-strained nanostructures using cross-sectional scanning tunneling microscopy and showed that tunable, defect-free self-assembly is
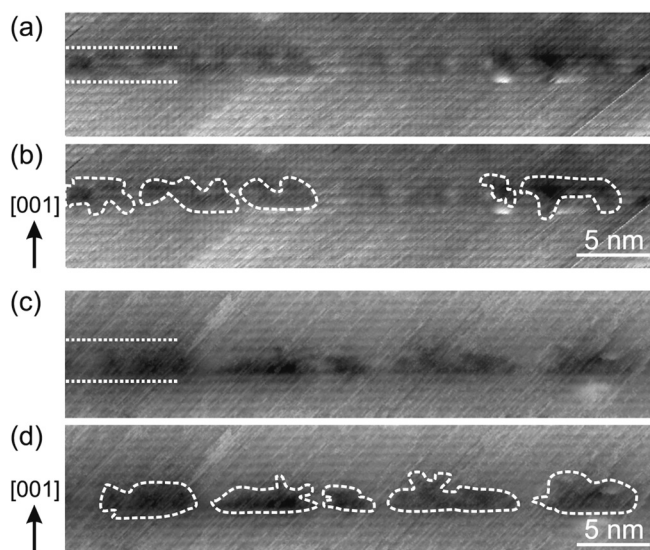
FIG. 20. Cross-sectional scanning tunneling microscope (XSTM) images of (a) and (b) 1 ML and (c) and (d) 2 ML GaAs/GaSb(001) QDs. (a) and (b) Empty-state and (c) and (d) filled-state XSTM images. In (a) and (c), the height of the GaAs containing layer is indicated by the dotted lines; in (b) and (d), the GaAs nanostructures are indicated by dashed lines. Reprinted with permission from Lenz et al., Appl. Phys. Lett. **102**, 102105 (2013). Copyright 2013 AIP Publishing LLC.[232]

possible in that system (Fig. 20).[232] Zhang et al. and Huo et al. demonstrated Ge(001) QDs grown on various III–V semiconductors, but either did not show if these QDs were defect-free[194] or found that there was anti-phase disorder in the capping layer.[248] Pachinger et al. demonstrated Si QDs grown on Ge(001), but these QDs were dislocated.[249] All of these examples demonstrate the breadth of research into developing new, tensile-based QDs for a range of future technologies.

VII. CONCLUSIONS

In this tutorial, we have explored the mechanisms, materials systems, and applications of semiconductor QDs grown by MBE using strain-driven self-assembly. We outlined the history of this field, from the earliest attempts at creating 3D QWs, right up to highly symmetric QDs designed specifically for future quantum information applications. There has been enormous progress made over the last 30 years, but new developments, such as the development of tensile-strained self-assembly, continue to push this important field forward. We hope that this tutorial will serve as an incomplete but useful guide. Perhaps collating some of the most frequently used MBE conditions for QD growth in one place will contribute to future efforts to create novel self-assembled QDs, with unique properties, for new applications.

AUTHORS' CONTRIBUTIONS

K.E.S. and K.D.V. contributed equally to this work.

DATA AVAILABILITY

The data that support the findings of this study are available from the corresponding author upon reasonable request.

REFERENCES

[1]A. Cho, "Film deposition by molecular-beam techniques," J. Vac. Sci. Technol. **8**, S31 (1971).

[2]L. L. Chang, L. Esaki, and R. Tsu, "Resonant tunneling in semiconductor double barriers," Appl. Phys. Lett. **24**, 593–595 (1974).

[3]R. Dingle, W. Wiegmann, and C. H. Henry, "Quantum states of confined carriers in very thin $Al_xGa_{1-x}As$-GaAs-$Al_xGa_{1-x}As$ heterostructures," Phys. Rev. Lett. **33**, 827–830 (1974).

[4]K. Kash, A. Scherer, J. Worlock, H. Craighead, and M. Tamargo, "Optical spectroscopy of ultrasmall structures etched from quantum wells," Appl. Phys. Lett. **49**, 1043–1045 (1986).

[5]H. Temkin, G. Dolan, M. Panish, and S. Chu, "Low-temperature photoluminescence from InGaAs/InP quantum wires and boxes," Appl. Phys. Lett. **50**, 413–415 (1987).

[6]M. Reed, J. Randall, R. Aggarwal, R. Matyi, T. Moore, and A. Wetsel, "Observation of discrete electronic states in a zero-dimensional semiconductor nanostructure," Phys. Rev. Lett. **60**, 535 (1988).

[7]T. Thornton, M. Pepper, H. Ahmed, D. Andrews, and G. Davies, "One-dimensional conduction in the 2D electron gas of a GaAs-AlGaAs heterojunction," Phys. Rev. Lett. **56**, 1198 (1986).

[8]D. Wharam, T. J. Thornton, R. Newbury, M. Pepper, H. Ahmed, J. Frost, D. Hasko, D. Peacock, D. Ritchie, and G. Jones, "One-dimensional transport and the quantisation of the ballistic resistance," J. Phys. C: Solid State Phys. **21**, L209 (1988).

[9]B. Van Wees, H. Van Houten, C. Beenakker, J. G. Williamson, L. Kouwenhoven, D. Van der Marel, and C. Foxon, "Quantized conductance of point contacts in a two-dimensional electron gas," Phys. Rev. Lett. **60**, 848 (1988).

[10]P. Simmonds, F. Sfigakis, H. Beere, D. Ritchie, M. Pepper, D. Anderson, and G. Jones, "Quantum transport in $In_{0.75}Ga_{0.25}As$ quantum wires," Appl. Phys. Lett. **92**, 152108 (2008).

[11]U. Meirav, M. Kastner, and S. Wind, "Single-electron charging and periodic conductance resonances in gaas nanostructures," Phys. Rev. Lett. **65**, 771 (1990).

[12]A. Johnson, L. Kouwenhoven, W. De Jong, N. Van der Vaart, C. Harmans, and C. Foxon, "Zero-dimensional states and single electron charging in quantum dots," Phys. Rev. Lett. **69**, 1592 (1992).

[13]R. Ashoori, "Electrons in artificial atoms," Nature **379**, 413–419 (1996).

[14]M. Grundmann, J. Christen, N. Ledentsov, J. Böhrer, D. Bimberg, S. Ruvimov, P. Werner, U. Richter, U. Gösele, J. Heydenreich et al., "Ultranarrow luminescence lines from single quantum dots," Phys. Rev. Lett. **74**, 4043 (1995).

[15]W. Schaffer, M. Lind, S. Kowalczyk, and R. Grant, "Nucleation and strain relaxation at the InAs/GaAs (100) heterojunction," J. Vac. Sci. Technol. B **1**, 688–695 (1983).

[16]B. Elman, E. S. Koteles, P. Melman, C. Jagannath, J. Lee, and D. Dugger, "In situ measurements of critical layer thickness and optical studies of InGaAs quantum wells grown on GaAs substrates," Appl. Phys. Lett. **55**, 1659–1661 (1989).

[17]Y. Kataoka, H. Ueba, and C. Tatsuyama, "Structural properties of heteroepitaxial Ge films on a Si (100)-2×1 surface," J. Appl. Phys. **63**, 749–759 (1988).

[18]M. Copel, M. Reuter, E. Kaxiras, and R. Tromp, "Surfactants in epitaxial growth," Phys. Rev. Lett. **63**, 632 (1989).

[19]F. LeGoues, M. Copel, and R. Tromp, "Novel strain-induced defect in thin molecular-beam epitaxy layers," Phys. Rev. Lett. **63**, 1826 (1989).

[20]H. Nakao and T. Yao, "Surface lattice strain relaxation at the initial stage of heteroepitaxial growth of $In_xGa_{1-x}As$ on GaAs by molecular beam epitaxy," Jpn. J. Appl. Phys. **28**, L352 (1989).

[21]J.-P. Reithmaier, H. Cerva, and R. Lösch, "Investigation of the critical layer thickness in elastically strained InGaAs/GaAlAs quantum wells by photoluminescence and transmission electron microscopy," Appl. Phys. Lett. **54**, 48–50 (1989).

[22]C. Snyder, B. Orr, D. Kessler, and L. Sander, "Effect of strain on surface morphology in highly strained InGaAs films," Phys. Rev. Lett. **66**, 3032 (1991).

[23]S. Guha, A. Madhukar, and K. Rajkumar, "Onset of incoherency and defect introduction in the initial stages of molecular beam epitaxial growth of highly strained $In_xGa_{1-x}As$ on GaAs(100)," Appl. Phys. Lett. **57**, 2110–2112 (1990).

[24]D. Eaglesham and M. Cerullo, "Dislocation-free Stranski-Krastanow growth of Ge on Si(100)," Phys. Rev. Lett. **64**, 1943 (1990).

[25]M. Krishnamurthy, J. Drucker, and J. Venables, "Microstructural evolution during the heteroepitaxy of Ge on vicinal Si(100)," J. Appl. Phys. **69**, 6461–6471 (1991).

[26]D. Leonard, M. Krishnamurthy, C. M. Reaves, S. P. DenBaars, and P. M. Petroff, "Direct formation of quantum-sized dots from uniform coherent islands of InGaAs on GaAs surfaces," Appl. Phys. Lett. **63**, 3203–3205 (1993).

[27]J. Moison, F. Houzay, F. Barthe, L. Leprince, E. Andre, and O. Vatel, "Self-organized growth of regular nanometer-scale InAs dots on GaAs," Appl. Phys. Lett. **64**, 196–198 (1994).

[28]J. Marzin and J. Gerard, "Optical properties of some III–V strained-layer superlattices," Superlattices Microstruct. **5**, 51–58 (1989).

[29]K. Mukai, N. Ohtsuka, M. Sugawara, and S. Yamazaki, "Self-formed $In_{0.5}Ga_{0.5}As$ quantum dots on GaAs substrates emitting at $1.3\,\mu m$," Jpn. J. Appl. Phys. **33**, L1710 (1994).

[30]Y. Nabetani, T. Ishikawa, S. Noda, and A. Sasaki, "Initial growth stage and optical properties of a three-dimensional InAs structure on GaAs," J. Appl. Phys. **76**, 347–351 (1994).

[31]D. Leonard, M. Krishnamurthy, S. Fafard, J. Merz, and P. Petroff, "Molecular beam epitaxy growth of quantum dots from strained coherent uniform islands of InGaAs on GaAs," J. Vac. Sci. Technol. B **12**, 1063–1066 (1994).

[32]Q. Xie, P. Chen, A. Kalburge, T. Ramachandran, A. Nayfonov, A. Konkar, and A. Madhukar, "Realization of optically active strained InAs island quantum boxes on GaAs (100) via molecular beam epitaxy and the role of island induced strain fields," J. Cryst. Growth **150**, 357–363 (1995).

[33]J.-M. Gérard, J. Genin, J. Lefebvre, J. Moison, N. Lebouche, and F. Barthe, "Optical investigation of the self-organized growth of InAs/GaAs quantum boxes," J. Cryst. Growth **150**, 351–356 (1995).

[34]D. Bimberg, M. Grundmann, N. Ledentsov, S. Ruvimov, P. Werner, U. Richter, J. Heydenreich, V. Ustinov, P. Kop'ev, and Z. I. Alferov, "Self-organization processes in MBE-grown quantum dot structures," Thin Solid Films **267**, 32–36 (1995).

[35]N. Ledentsov, V. Shchukin, M. Grundmann, N. Kirstaedter, J. Böhrer, O. Schmidt, D. Bimberg, V. Ustinov, A. Y. Egorov, A. Zhukov et al., "Direct formation of vertically coupled quantum dots in Stranski-Krastanow growth," Phys. Rev. B **54**, 8743 (1996).

[36]F. Hatami, N. Ledentsov, M. Grundmann, J. Böhrer, F. Heinrichsdorff, M. Beer, D. Bimberg, S. Ruvimov, P. Werner, U. Gösele et al., "Radiative recombination in type-II GaSb/GaAs quantum dots," Appl. Phys. Lett. **67**, 656–658 (1995).

[37]E. Glaser, B. Bennett, B. Shanabrook, and R. Magno, "Photoluminescence studies of self-assembled InSb, GaSb, and AlSb quantum dot heterostructures," Appl. Phys. Lett. **68**, 3614–3616 (1996).

[38]B. Junno, T. Junno, M. Miller, and L. Samuelson, "A reflection high-energy electron diffraction and atomic force microscopy study of the chemical beam epitaxial growth of InAs and InP islands on (001) GaP," Appl. Phys. Lett. **72**, 954–956 (1998).

[39]S. Gerhard, V. Baumann, S. Höfling, and A. Forchel, "The structural and optical characterization of high areal density $Ga_xIn_{1-x}P$ quantum dots on GaP," Nanotechnology **20**, 434016 (2009).

[40]F. Hatami, W. Masselink, and L. Schrottke, "Radiative recombination from InP quantum dots on (100) GaP," Appl. Phys. Lett. **78**, 2163–2165 (2001).

[41]S. Fafard, Z. Wasilewski, J. McCaffrey, S. Raymond, and S. Charbonneau, "InAs self-assembled quantum dots on InP by molecular beam epitaxy," Appl. Phys. Lett. **68**, 991–993 (1996).

[42]V. M. Ustinov, E. R. Weber, S. Ruvimov, Z. Liliental-Weber, A. E. Zhukov, A. Y. Egorov, A. R. Kovsh, A. F. Tsatsul'nikov, and P. S. Kop'ev, "Effect of matrix on InAs self-organized nanostructures on InP substrate," Appl. Phys. Lett. **72**, 362–364 (1998).

[43]B. Lambert, A. Le Corre, V. Drouot, H. L'Haridon, and S. Loualiche, "High photoluminescence efficiency of InAs/InP self-assembled quantum dots emitting at 1.5-1.6 μm," Semicond. Sci. Technol. **13**, 143–145 (1998).

[44]Y. Song, P. J. Simmonds, and M. L. Lee, "Self-assembled $In_{0.5}Ga_{0.5}As$ quantum dots on GaP," Appl. Phys. Lett. **97**, 223110 (2010).

[45]D. Huang, M. A. Reshchikov, and H. Morkoç, "Growth, structures, and optical properties of III-nitride quantum dots," Int. J. High Speed Electron. Syst. **12**, 79–110 (2002).

[46]X.-Q. Shen, S. Tanaka, S. Iwai, and Y. Aoyagi, "The formation of GaN dots on Al_xGa_{1-x}n surfaces using Si in gas-source molecular beam epitaxy," Appl. Phys. Lett. **72**, 344–346 (1998).

[47]S. P. Minor, "Growth of indium nitride quantum dots by molecular beam epitaxy," Ph.D. thesis (University of Arkansas, Fayetteville, 2019).

[48]C. Adelmann, J. Simon, G. Feuillet, N. Pelekanos, B. Daudin, and G. Fishman, "Self-assembled InGaN quantum dots grown by molecular-beam epitaxy," Appl. Phys. Lett. **76**, 1570–1572 (2000).

[49]S. Xin, P. Wang, A. Yin, C. Kim, M. Dobrowolska, J. Merz, and J. Furdyna, "Formation of self-assembling CdSe quantum dots on ZnSe by molecular beam epitaxy," Appl. Phys. Lett. **69**, 3884–3886 (1996).

[50]I. Hernaíndez-Calderoín, "Epitaxial growth of thin films and quantum structures of II–VI visible-bandgap semiconductors," in *Molecular Beam Epitaxy: From Research to Mass Production*, edited by M. Henini (Elsevier, 2013), p. 311.

[51]P. Wojnar, Ł. Kłopotowski, and J. Kossut, "Molecular beam epitaxy of semi-magnetic quantum dots," in *Molecular Beam Epitaxy: From Research to Mass Production*, edited by M. Henini (Elsevier, 2013), pp. 529–545.

[52]G. Karczewski, S. Maćkowski, M. Kutrowski, T. Wojtowicz, and J. Kossut, "Photoluminescence study of CdTe/ZnTe self-assembled quantum dots," Appl. Phys. Lett. **74**, 3011–3013 (1999).

[53]P. Simmonds and M. L. Lee, "Tensile strained island growth at step-edges on GaAs (110)," Appl. Phys. Lett. **97**, 153101 (2010).

[54]P. J. Simmonds and M. L. Lee, "Self-assembly on (111)-oriented III-V surfaces," Appl. Phys. Lett. **99**, 123111 (2011).

[55]P. J. Simmonds and M. L. Lee, "Tensile-strained growth on low-index GaAs," J. Appl. Phys. **112**, 054313 (2012).

[56]P. J. Simmonds, C. D. Yerino, M. Sun, B. Liang, D. L. Huffaker, V. G. Dorogan, Y. Mazur, G. Salamo, and M. L. Lee, "Tuning quantum dot luminescence below the bulk band gap using tensile strain," ACS Nano **7**, 5017–5023 (2013).

[57]C. D. Yerino, P. J. Simmonds, B. Liang, V. G. Dorogan, M. E. Ware, Y. I. Mazur, D. Jung, D. L. Huffaker, G. J. Salamo, and M. L. Lee, "Tensile GaAs (111) quantum dashes with tunable luminescence below the bulk bandgap," Appl. Phys. Lett. **105**, 071912 (2014).

[58]C. D. Yerino, P. J. Simmonds, B. Liang, D. Jung, C. Schneider, S. Unsleber, M. Vo, D. L. Huffaker, S. Höfling, M. Kamp et al., "Strain-driven growth of GaAs(111) quantum dots with low fine structure splitting," Appl. Phys. Lett. **105**, 251901 (2014).

[59]C. F. Schuck, R. A. McCown, A. Hush, A. Mello, S. Roy, J. W. Spinuzzi, B. Liang, D. L. Huffaker, and P. J. Simmonds, "Self-assembly of (111)-oriented tensile-strained quantum dots by molecular beam epitaxy," J. Vac. Sci. Technol. B **36**, 031803 (2018).

[60]C. F. Schuck, S. K. Roy, T. Garrett, Q. Yuan, Y. Wang, C. I. Cabrera, K. A. Grossklaus, T. E. Vandervelde, B. Liang, and P. J. Simmonds, "Anomalous Stranski-Krastanov growth of (111)-oriented quantum dots with tunable wetting layer thickness," Sci. Rep. **9**, 18179 (2019).

[61]C. E. Pryor and M.-E. Pistol, "Band-edge diagrams for strained III-V semiconductor quantum wells, wires, and dots," Phys. Rev. B **72**, 205311 (2005).

[62]P. G. Eliseev, H. Li, G. T. Liu, A. Stintz, T. C. Newell, L. F. Lester, and K. J. Malloy, "Ground-state emission and gain in ultralow-threshold InAs-InGaAs quantum-dot lasers," IEEE J. Sel. Top. Quantum Electron. **7**, 135–142 (2001).

[63]B. Ellis, M. A. Mayer, G. Shambat, T. Sarmiento, J. Harris, E. E. Haller, and J. Vučković, "Ultralow-threshold electrically pumped quantum-dot photonic-crystal nanocavity laser," Nat. Photonics **5**, 297–300 (2011).

[64]T. Zhou, M. Tang, G. Xiang, X. Fang, X. Liu, B. Xiang, S. Hark, M. Martin, M.-L. Touraton, T. Baron, Y. Lu, S. Chen, H. Liu, and Z. Zhang, "Ultra-low threshold InAs/GaAs quantum dot microdisk lasers on planar on-axis Si (001) substrates," Optica **6**, 430–435 (2019).

[65]C. H. Bennet and G. Brassard, "Quantum cryptography: Public key distribution and coin tossing," in *Proceedings IEEE International Conference on Computers, Systems and Signal Processing* (IEEE, New York, 1984), p. 175.

[66]A. Schliwa, M. Winkelnkemper, A. Lochmann, E. Stock, and D. Bimberg, "In (Ga)As/GaAs quantum dots grown on a (111) surface as ideal sources of entangled photon pairs," Phys. Rev. B **80**, 161307 (2009).

[67]A. Shields, "Quantum logic with light, glass, and mirrors," Science **297**, 1821 (2002).

[68]A. J. Shields, "Semiconductor quantum light sources," Nat. Photonics **1**, 215–223 (2007).

[69]N. Gisin, G. Ribordy, W. Tittel, and H. Zbinden, "Quantum cryptography," Rev. Mod. Phys. **74**, 145 (2002).

[70]N. Gisin and R. Thew, "Quantum communication," Nat. Photonics **1**, 165–171 (2007).

[71]M. D. Eisaman, J. Fan, A. Migdall, and S. V. Polyakov, "Invited review article: Single-photon sources and detectors," Rev. Sci. Instrum. **82**, 071101 (2011).

[72]J.-H. Kim, S. Aghaeimeibodi, J. Carolan, D. Englund, and E. Waks, "Hybrid integration methods for on-chip quantum photonics," Optica **7**, 291–308 (2020).

[73]C. Santori, M. Pelton, G. Solomon, Y. Dale, and Y. Yamamoto, "Triggered single photons from a quantum dot," Phys. Rev. Lett. **86**, 1502–1505 (2001).

[74]J. Claudon, J. Bleuse, N. S. Malik, M. Bazin, P. Jaffrennou, N. Gregersen, C. Sauvan, P. Lalanne, and J.-M. Gérard, "A highly efficient single-photon source based on a quantum dot in a photonic nanowire," Nat. Photonics **4**, 174–177 (2010).

[75]K. Rivoire, S. Buckley, Y. Song, M. L. Lee, and J. Vučković, "Photoluminescence from In$_{0.5}$Ga$_{0.5}$As/GaP quantum dots coupled to photonic crystal cavities," Phys. Rev. B **85**, 045319 (2012).

[76]S. Unsleber, M. Deppisch, C. M. Krammel, M. Vo, C. D. Yerino, P. J. Simmonds, M. L. Lee, P. M. Koenraad, C. Schneider, and S. Höfling, "Bulk AlInAs on InP (111) as a novel material system for pure single photon emission," Opt. Express **24**, 23198–23206 (2016).

[77]H. Paul, "Photon antibunching," Rev. Mod. Phys. **54**, 1061–1102 (1982).

[78]R. P. Mirin, "Photon antibunching at high temperature from a single InGaAs/GaAs quantum dot," Appl. Phys. Lett. **84**, 1260–1262 (2004).

[79]R. Hanbury Brown and R. Q. Twiss, "Correlation between photons in two coherent beams of light," Nature **177**, 27–29 (1956).

[80]A. K. Ekert, "Quantum cryptography based on Bell's theorem," Phys. Rev. Lett. **67**, 661–663 (1991).

[81]J. Rarity, P. Owens, and P. Tapster, "Quantum random-number generation and key sharing," J. Mod. Opt. **41**, 2435–2444 (1994).

[82]K. R. Motes, J. P. Olson, E. J. Rabeaux, J. P. Dowling, S. J. Olson, and P. P. Rohde, "Linear optical quantum metrology with single photons: Exploiting spontaneously generated entanglement to beat the shot-noise limit," Phys. Rev. Lett. **114**, 170802 (2015).

[83]C. Gobby, Z. L. Yuan, and A. J. Shields, "Quantum key distribution over 122 km of standard telecom fiber," Appl. Phys. Lett. **84**, 3762–3764 (2004).

[84]M. A. Jaspan, J. L. Habif, R. H. Hadfield, and S. W. Nam, "Heralding of telecommunication photon pairs with a superconducting single photon detector," Appl. Phys. Lett. **89**, 031112 (2006).

[85]R. H. Hadfield, "Single-photon detectors for optical quantum information applications," Nat. Photonics **3**, 696–705 (2009).

[86]C. M. Natarajan, M. G. Tanner, and R. H. Hadfield, "Superconducting nanowire single-photon detectors: Physics and applications," Supercond. Sci. Technol. **25**, 063001 (2012).

[87]S. Komiyama, O. Astafiev, V. Antonov, T. Kutsuwa, and H. Hirai, "A single-photon detector in the far-infrared range," Nature **403**, 405–407 (2000).

[88]A. J. Shields, M. P. O'Sullivan, I. Farrer, D. A. Ritchie, M. L. Leadbeater, N. K. Patel, R. A. Hogg, C. E. Norman, N. J. Curson, and M. Pepper, "Single photon detection with a quantum dot transistor," Jpn. J. Appl. Phys. **40**, 2058–2064 (2001).

[89]B. E. Kardynal, A. J. Shields, M. P. O'Sullivan, N. S. Beattie, I. Farrer, D. A. Ritchie, and K. Cooper, "Detection of single photons using a field effect transistor with a layer of quantum dots," Meas. Sci. Technol. **13**, 1721–1726 (2002).

[90]J. C. Blakesley, P. See, A. J. Shields, B. E. Kardynal, P. Atkinson, I. Farrer, and D. A. Ritchie, "Efficient single photon detection by quantum dot resonant tunneling diodes," Phys. Rev. Lett. **94**, 067401 (2005).

[91]M. A. Rowe, E. J. Gansen, M. Greene, R. H. Hadfield, T. E. Harvey, M. Y. Su, S. W. Nam, R. P. Mirin, and D. Rosenberg, "Single-photon detection using a quantum dot optically gated field-effect transistor with high internal quantum efficiency," Appl. Phys. Lett. **89**, 253505 (2006).

[92]H. W. Li, B. E. Kardynał, P. See, A. J. Shields, P. Simmonds, H. E. Beere, and D. A. Ritchie, "Quantum dot resonant tunneling diode for telecommunication wavelength single photon detection," Appl. Phys. Lett. **91**, 073516 (2007).

[93]Q. Weng, Z. An, B. Zhang, P. Chen, X. Chen, Z. Zhu, and W. Lu, "Quantum dot single-photon switches of resonant tunneling current for discriminating-photon-number detection," Sci. Rep. **5**, 9389 (2015).

[94]D. Bouwmeester, J.-W. Pan, K. Mattle, M. Eibl, H. Weinfurter, and A. Zeilinger, "Experimental quantum teleportation," Nature **390**, 575–579 (1997).

[95]O. Benson, C. Santori, M. Pelton, and Y. Yamamoto, "Regulated and entangled photons from a single quantum dot," Phys. Rev. Lett. **84**, 2513–2516 (2000).

[96]P. G. Kwiat, K. Mattle, H. Weinfurter, A. Zeilinger, A. V. Sergienko, and Y. Shih, "New high-intensity source of polarization-entangled photon pairs," Phys. Rev. Lett. **75**, 4337–4341 (1995).

[97]K. Edamatsu, G. Oohata, R. Shimizu, and T. Itoh, "Generation of ultraviolet entangled photons in a semiconductor," Nature **431**, 167–170 (2004).

[98]J. K. Thompson, J. Simon, H. Loh, and V. Vuletić, "A high-brightness source of narrowband, identical-photon pairs," Science **313**, 74–77 (2006).

[99]J. Fulconis, O. Alibart, J. L. O'Brien, W. J. Wadsworth, and J. G. Rarity, "Nonclassical interference and entanglement generation using a photonic crystal fiber pair photon source," Phys. Rev. Lett. **99**, 120501 (2007).

[100]B. Hacker, S. Welte, G. Rempe, and S. Ritter, "A photon-photon quantum gate based on a single atom in an optical resonator," Nature **536**, 193–196 (2016).

[101]Z. Yuan, B. E. Kardynal, R. M. Stevenson, A. J. Shields, C. J. Lobo, K. Cooper, N. S. Beattie, D. A. Ritchie, and M. Pepper, "Electrically driven single-photon source," Science **295**, 102–105 (2002).

[102]T. Heindel, C. Schneider, M. Lermer, S. H. Kwon, T. Braun, S. Reitzenstein, S. Höfling, M. Kamp, and A. Forchel, "Electrically driven quantum dot-micropillar single photon source with 34% overall efficiency," Appl. Phys. Lett. **96**, 011107 (2010).

[103]R. M. Stevenson, R. J. Young, P. Atkinson, K. Cooper, D. A. Ritchie, and A. J. Shields, "A semiconductor source of triggered entangled photon pairs," Nature **439**, 179–182 (2006).

[104]N. Akopian, N. H. Lindner, E. Poem, Y. Berlatzky, J. Avron, D. Gershoni, B. D. Gerardot, and P. M. Petroff, "Entangled photon pairs from semiconductor quantum dots," Phys. Rev. Lett. **96**, 130501 (2006).

[105]R. Hafenbrak, S. M. Ulrich, P. Michler, L. Wang, A. Rastelli, and O. G. Schmidt, "Triggered polarization-entangled photon pairs from a single quantum dot up to 30 K," New J. Phys. **9**, 315 (2007).

[106]R. Seguin, A. Schliwa, S. Rodt, K. Pötschke, U. Pohl, and D. Bimberg, "Size-dependent fine-structure splitting in self-organized InAs/GaAs quantum dots," Phys. Rev. Lett. **95**, 257402 (2005).

[107]D. Gammon, E. S. Snow, B. V. Shanabrook, D. S. Katzer, and D. Park, "Fine structure splitting in the optical spectra of single GaAs quantum dots," Phys. Rev. Lett. **76**, 3005–3008 (1996).

[108]D. J. P. Ellis, R. M. Stevenson, R. J. Young, A. J. Shields, P. Atkinson, and D. A. Ritchie, "Control of fine-structure splitting of individual InAs quantum dots by rapid thermal annealing," Appl. Phys. Lett. **90**, 011907 (2007).

[109]M. A. Pooley, A. J. Bennett, I. Farrer, D. A. Ritchie, and A. J. Shields, "Engineering quantum dots for electrical control of the fine structure splitting," Appl. Phys. Lett. **103**, 031105 (2013).

[110]C. Varnava, R. M. Stevenson, J. Nilsson, J. Skiba-Szymanska, B. Dzurňák, M. Lucamarini, R. V. Penty, I. Farrer, D. A. Ritchie, and A. J. Shields, "An entangled-LED-driven quantum relay over 1 km," npj Quantum Inf. **2**, 16006 (2016).

[111]T. Müller, J. Skiba-Szymanska, A. B. Krysa, J. Huwer, M. Felle, M. Anderson, R. M. Stevenson, J. Heffernan, D. A. Ritchie, and A. J. Shields, "A quantum light-emitting diode for the standard telecom window around 1,550 nm," Nat. Commun. **9**, 862 (2018).

[112]N. Ha, T. Mano, T. Kuroda, Y. Sakuma, and K. Sakoda, "Current-injection quantum-entangled-pair emitter using droplet epitaxial quantum dots on GaAs (111)A," Appl. Phys. Lett. **115**, 083106 (2019).

[113]N. Koguchi, S. Takahashi, and T. Chikyow, "New MBE growth method for InSb quantum well boxes," J. Cryst. Growth **111**, 688–692 (1991).

[114]F. Ratto and F. Rosei, "Order and disorder in the heteroepitaxy of semiconductor nanostructures," Mater. Sci. Eng. R. Rep. **70**, 243–264 (2010).

[115]Lateral Alignment of Epitaxial Quantum Dots, edited by O. G. Schmidt (Springer-Verlag, Berlin, 2007).

[116]N. Koguchi and K. Ishige, "Growth of GaAs epitaxial microcrystals on an S-terminated GaAs substrate by successive irradiation of Ga and As molecular beams," Jpn. J. Appl. Phys. **32**, 2052 (1993).

[117]K. Watanabe, N. Koguchi, and Y. Gotoh, "Fabrication of GaAs quantum dots by modified droplet epitaxy," Jpn. J. Appl. Phys. **39**, L79–L81 (2000).

[118]C. Heyn, A. Stemmann, A. Schramm, H. Welsch, W. Hansen, and Á. Nemcsics, "Regimes of GaAs quantum dot self-assembly by droplet epitaxy," Phys. Rev. B **76**, 075317 (2007).

[119]B. Liang, A. Lin, N. Pavarelli, C. Reyner, J. Tatebayashi, K. Nunna, J. He, T. J. Ochalski, G. Huyet, and D. L. Huffaker, "GaSb/GaAs type-II quantum dots grown by droplet epitaxy," Nanotechnology **20**, 455604 (2009).

[120]Z. M. Wang, B. Liang, K. A. Sablon, J. Lee, Y. I. Mazur, N. W. Strom, and G. J. Salamo, "Self-organization of InAs quantum-dot clusters directed by droplet homoepitaxy," Small **3**, 235–238 (2007).

[121]M. Gurioli, Z. Wang, A. Rastelli, T. Kuroda, and S. Sanguinetti, "Droplet epitaxy of semiconductor nanostructures for quantum photonic devices," Nat. Mater. **18**, 799–810 (2019).

[122]J. Wu and Z. M. Wang, "Droplet epitaxy for advanced optoelectronic materials and devices," J. Phys. D: Appl. Phys. **47**, 173001 (2014).

[123]E. Bauer, "Phänomenologische theorie der kristallabscheidung an oberflächen. I," Z. Kristallogr. Cryst. Mater. **110**, 372–394 (1958).

[124]R. Heckingbottom, "The application of thermodynamics to molecular beam epitaxy," in Molecular Beam Epitaxy and Heterostructures, edited by L. L. Chang and K. Ploog (Springer Netherlands, Dordrecht, 1985), pp. 71–104.

[125]B. Joyce and D. Vvedensky, "Self-organized growth on GaAs surfaces," Mater. Sci. Eng. R **46**, 127–176 (2004).

[126]M. I. Vesselinov, Crystal Growth for Beginners: Fundamentals of Nucleation, Crystal Growth and Epitaxy (World Scientific, 2016).

[127]T. J. Krzyzewski and T. S. Jones, "Ripening and annealing effects in InAs/GaAs(001) quantum dot formation," J. Appl. Phys. **96**, 668–674 (2004).

[128]J. W. Evans, P. A. Thiel, and M. C. Bartelt, "Morphological evolution during epitaxial thin film growth: Formation of 2D islands and 3D mounds," Surf. Sci. Rep. **61**, 1–128 (2006).

[129]R. L. Schwoebel and E. J. Shipsey, "Step motion on crystal surfaces," J. Appl. Phys. **37**, 3682–3686 (1966).

[130]U. Pohl, Epitaxy of Semiconductors: Introduction to Physical Principles, Graduate Texts in Physics (Springer, Berlin, 2013).

[131]B. Mutaftschiev, The Atomistic Nature of Crystal Growth, Springer Series in Materials Science (Springer, Berlin, 2013).

[132]K. Nakajima, "Equilibrium phase diagrams for Stranski-Krastanov structure mode of III–V ternary quantum dots," Jpn. J. Appl. Phys. **38**, 1875–1883 (1999).

[133]T. Moustakas, T. Xu, C. Thomidis, A. Y. Nikiforov, L. Zhou, and D. J. Smith, "Growth of III-nitride quantum dots and their applications to blue-green LEDs," Phys. Status Solidi A **205**, 2560–2565 (2008).

[134]A.-L. Barabási, "Thermodynamic and kinetic mechanisms in self-assembled quantum dot formation," Mater. Sci. Eng. B **67**, 23–30 (1999).

[135]D. K. Biegelsen, F. A. Ponce, A. J. Smith, and J. C. Tramontana, "Initial stages of epitaxial growth of GaAs on (100) silicon," J. Appl. Phys. **61**, 1856–1859 (1987).

[136]R. Hull and A. Fischer-Colbrie, "Nucleation of GaAs on Si: Experimental evidence for a three-dimensional critical transition," Appl. Phys. Lett. **50**, 851–853 (1987).

[137]A. Raviswaran, C.-P. Liu, J. Kim, D. G. Cahill, and J. M. Gibson, "Evolution of coherent islands during strained-layer Volmer-Weber growth of Si on Ge (111)," Phys. Rev. B **63**, 125314 (2001).

[138]A. Ponchet, G. Patriarche, J. B. Rodriguez, L. Cerutti, and E. Tournié, "Interface energy analysis of III-V islands on Si (001) in the Volmer-Weber growth mode," Appl. Phys. Lett. **113**, 191601 (2018).

[139]K. E. Sautter, C. F. Schuck, T. A. Garrett, A. E. Weltner, K. D. Vallejo, D. Ren, B. Liang, K. A. Grossklaus, T. E. Vandervelde, and P. J. Simmonds, "Self-assembly of tensile-strained Ge quantum dots on InAlAs(111)A," J. Cryst. Growth **533**, 125468 (2020).

[140]K. Lozovoy, A. Kokhanenko, and A. Voitsekhovskii, "Comparative analysis of germanium–silicon quantum dots formation on Si(100), Si(111) and Sn/Si(100) surfaces," Nanotechnology **29**, 054002 (2018).

[141]R. Fornari, "Epitaxy for energy materials," in Handbook of Crystal Growth, 2nd ed., Handbook of Crystal Growth, edited by T. F. Kuech (North-Holland, Boston, 2015), Chap. 1, pp. 1–49.

[142]P. M. Petroff, "Epitaxial growth and electronic structure of self-assembled quantum dots," in Single Quantum Dots (Springer, 2003), pp. 1–24.

[143]J. Tersoff and F. LeGoues, "Competing relaxation mechanisms in strained layers," Phys. Rev. Lett. **72**, 3570 (1994).

[144]A. Cullis, D. Norris, T. Walther, M. Migliorato, and M. Hopkinson, "Stranski-Krastanow transition and epitaxial island growth," Phys. Rev. B **66**, 081305 (2002).

[145]Y. Tu and J. Tersoff, "Origin of apparent critical thickness for island formation in heteroepitaxy," Phys. Rev. Lett. **93**, 216101 (2004).

[146]T. Walther, A. G. Cullis, D. J. Norris, and M. Hopkinson, "Nature of the Stranski-Krastanow transition during epitaxy of InGaAs on GaAs," Phys. Rev. Lett. **86**, 2381–2384 (2001).

[147]H. Brune, "Growth modes," Technical Report, Pergamon, 2001.

[148]H. Li, J. Wu, B. Xu, J. Liang, and Z. Wang, "Ordered InAs quantum dots in InAlAs matrix on (001) InP substrates grown by molecular beam epitaxy," Appl. Phys. Lett. **72**, 2123–2125 (1998).

[149]P. J. Simmonds, H. E. Beere, H. W. Li, P. See, A. J. Shields, and D. A. Ritchie, "Growth by molecular beam epitaxy of self-assembled InAs quantum dots on InAlAs and InGaAs lattice-matched to InP," J. Vac. Sci. Technol. B **25**, 1044–1048 (2007).

[150]H. Eisele and M. Dähne, "Critical thickness of the 2-dimensional to 3-dimensional transition in GaSb/GaAs(001) quantum dot growth," J. Cryst. Growth **338**, 103–106 (2012).

[151]A. Schliwa, G. M. O. Hönig, and D. Bimberg, "Electronic properties of III-V quantum dots," in Multi-band Effective Mass Approximations, Lecture Notes in Computational Science and Engineering (Springer, Cham, 2014), Vol. 94, pp. 57–85.

[152]B. Voigtländer, "Fundamental processes in Si/Si and Ge/Si epitaxy studied by scanning tunneling microscopy during growth," Surf. Sci. Rep. **43**, 127–254 (2001).

[153]Y.-W. Mo, D. Savage, B. Swartzentruber, and M. G. Lagally, "Kinetic pathway in Stranski-Krastanov growth of Ge on Si (001)," Phys. Rev. Lett. **65**, 1020 (1990).

[154]C. Teichert, "Self-organization of nanostructures in semiconductor heteroepitaxy," Phys. Rep. **365**, 335–432 (2002).

[155]M. L. Lee, C. W. Leitz, Z. Cheng, A. J. Pitera, T. Langdo, M. T. Currie, G. Taraschi, E. A. Fitzgerald, and D. A. Antoniadis, "Strained Ge channel p-type metal-oxide-semiconductor field-effect transistors grown on $Si_{1-x}Ge_x$/Si virtual substrates," Appl. Phys. Lett. **79**, 3344–3346 (2001).

[156]M. L. Lee, E. A. Fitzgerald, M. T. Bulsara, M. T. Currie, and A. Lochtefeld, "Strained Si, SiGe, and Ge channels for high-mobility metal-oxide-semiconductor field-effect transistors," J. Appl. Phys. **97**, 011101 (2005).

[157]F. M. Ross, R. Tromp, and M. Reuter, "Transition states between pyramids and domes during Ge/Si island growth," Science **286**, 1931–1934 (1999).

[158]B. Spencer and J. Tersoff, "Asymmetry and shape transitions of epitaxially strained islands on vicinal surfaces," Appl. Phys. Lett. **96**, 073114 (2010).

[159]I. Daruka, J. Tersoff, and A.-L. Barabási, "Shape transition in growth of strained islands," Phys. Rev. Lett. **82**, 2753 (1999).

[160]L. Persichetti, A. Sgarlata, M. Fanfoni, and A. Balzarotti, "Shaping Ge islands on Si (001) surfaces with misorientation angle," Phys. Rev. Lett. **104**, 036104 (2010).

[161]T. Zhou and Z. Zhong, "Dramatically enhanced self-assembly of GeSi quantum dots with superior photoluminescence induced by the substrate misorientation," APL Mater. **2**, 022108 (2014).

[162]M. Copel, M. Reuter, M. H. Von Hoegen, and R. Tromp, "Influence of surfactants in Ge and Si epitaxy on Si (001)," Phys. Rev. B **42**, 11682 (1990).

[163]K. Brunner, "Si/Ge nanostructures," Rep. Prog. Phys. **65**, 27 (2001).

[164]P. Joyce, T. Krzyzewski, G. Bell, B. Joyce, and T. Jones, "Composition of InAs quantum dots on GaAs (001): Direct evidence for (In, Ga) As alloying," Phys. Rev. B **58**, R15981 (1998).

[165]M. Yano, M. Nogami, Y. Matsushima, and M. Kimata, "Molecular beam epitaxial growth of InAs," Jpn. J. Appl. Phys. **16**, 2131 (1977).

[166]F. Houzay, C. Guille, J. Moison, P. Henoc, and F. Barthe, "First stages of the MBE growth of InAs on (001) GaAs," J. Cryst. Growth **81**, 67–72 (1987).

[167]I. Kegel, T. Metzger, A. Lorke, J. Peisl, J. Stangl, G. Bauer, J. Garcia, and P. Petroff, "Nanometer-scale resolution of strain and interdiffusion in self-assembled InAs/GaAs quantum dots," Phys. Rev. Lett. **85**, 1694 (2000).

[168]H.-M. Ji, B. Liang, P. J. Simmonds, B.-C. Juang, T. Yang, R. J. Young, and D. L. Huffaker, "Hybrid type-I InAs/GaAs and type-II GaSb/GaAs quantum dot structure with enhanced photoluminescence," Appl. Phys. Lett. **106**, 103104 (2015).

[169]O. Brandt, L. Tapfer, K. Ploog, R. Bierwolf, M. Hohenstein, F. Phillipp, H. Lage, and A. Heberle, "InAs quantum dots in a single-crystal GaAs matrix," Phys. Rev. B **44**, 8043 (1991).

[170]G. Wang, B. Liang, B.-C. Juang, A. Das, M. C. Debnath, D. L. Huffaker, Y. I. Mazur, M. E. Ware, and G. J. Salamo, "Comparative study of photoluminescence from $In_{0.3}Ga0.7As$/GaAs surface and buried quantum dots," Nanotechnology **27**, 465701 (2016).

[171]B. A. Joyce and D. D. Vvedensky, "Self-organized growth on GaAs surfaces," Mater. Sci. Eng. R. Rep. **46**, 127–176 (2004).

[172]C.-K. Sun, G. Wang, J. Bowers, B. Brar, H.-R. Blank, H. Kroemer, and M. Pilkuhn, "Optical investigations of the dynamic behavior of GaSb/GaAs quantum dots," Appl. Phys. Lett. **68**, 1543–1545 (1996).

[173]N. Grandjean, J. Massies, and V. Etgens, "Delayed relaxation by surfactant action in highly strained III-V semiconductor epitaxial layers," Phys. Rev. Lett. **69**, 796 (1992).

[174]K. Jacobi, "Atomic structure of InAs quantum dots on GaAs," Prog. Surf. Sci. **71**, 185–215 (2003).

[175]C. Heyn and W. Hansen, "Desorption of InAs quantum dots," J. Cryst. Growth **251**, 218–222 (2003).

[176]B. Ilahi, L. Sfaxi, F. Hassen, B. Salem, G. Bremond, O. Marty, L. Bouzaiene, and H. Maaref, "Optimizing the spacer layer thickness of vertically stacked InAs/GaAs quantum dots," Mater. Sci. Eng. C **26**, 374–377 (2006).

[177]R. Laghumavarapu, A. Moscho, A. Khoshakhlagh, M. El-Emawy, L. Lester, and D. Huffaker, "GaSb/GaAs type II quantum dot solar cells for enhanced infrared spectral response," Appl. Phys. Lett. **90**, 173125 (2007).

[178]K. Gradkowski, N. Pavarelli, T. J. Ochalski, D. P. Williams, J. Tatebayashi, G. Huyet, E. P. O'Reilly, and D. L. Huffaker, "Complex emission dynamics of type-II GaSb/GaAs quantum dots," Appl. Phys. Lett. **95**, 061102 (2009).

[179]K. Suzuki, R. A. Hogg, and Y. Arakawa, "Structural and optical properties of type II GaSb/GaAs self-assembled quantum dots grown by molecular beam epitaxy," J. Appl. Phys. **85**, 8349–8352 (1999).

[180]M. Sun, P. J. Simmonds, R. B. Laghumavarapu, A. Lin, C. J. Reyner, H.-S. Duan, B. Liang, and D. L. Huffaker, "Effects of GaAs(Sb) cladding layers on InAs/AlAsSb quantum dots," Appl. Phys. Lett. **102**, 023107 (2013).

[181]J. S. Kim, J. H. Lee, S. U. Hong, W. S. Han, H.-S. Kwack, C. W. Lee, and D. K. Oh, "Room-temperature operation of InP-based InAs quantum dot laser," IEEE Photonics Technol. Lett. **16**, 1607–1609 (2004).

[182]C. Paranthoen, N. Bertru, O. Dehaese, A. Le Corre, S. Loualiche, B. Lambert, and G. Patriarche, "Height dispersion control of InAs/InP quantum dots emitting at $1.55\,\mu m$," Appl. Phys. Lett. **78**, 1751–1753 (2001).

[183]J. Brault, M. Gendry, G. Grenet, G. Hollinger, Y. Desieres, and T. Benyattou, "Role of buffer surface morphology and alloying effects on the properties of InAs nanostructures grown on InP (001)," Appl. Phys. Lett. **73**, 2932–2934 (1998).

[184]J. Brault, M. Gendry, G. Grenet, G. Hollinger, J. Olivares, B. Salem, T. Benyattou, and G. Bremond, "Surface effects on shape, self-organization and photoluminescence of InAs islands grown on InAlAs/InP (001)," J. Appl. Phys. **92**, 506–510 (2002).

[185]A. Rudra, R. Houdré, J. Carlin, and M. Ilegems, "Dynamics of island formation in the growth of InAs/InP quantum wells," J. Cryst. Growth **136**, 278–281 (1994).

[186]L. González, J. García, R. García, F. Briones, J. Martínez-Pastor, and C. Ballesteros, "Influence of buffer-layer surface morphology on the self-organized growth of InAs on InP (001)nanostructures," Appl. Phys. Lett. **76**, 1104–1106 (2000).

[187]A. Weber, O. Gauthier-Lafaye, F. Julien, J. Brault, M. Gendry, Y. Desieres, and T. Benyattou, "Strong normal-incidence infrared absorption in self-organized InAs/InAlAs quantum dots grown on InP (001)," Appl. Phys. Lett. **74**, 413–415 (1999).

[188]H. Parry, M. Ashwin, J. Neave, and T. Jones, "Growth of InAs/InP(001) nanostructures: The transition from quantum wires to quantum dots," J. Cryst. Growth **278**, 131–135 (2005).

[189]R. H. Wang, A. Stintz, P. M. Varangis, T. C. Newell, H. Li, K. J. Malloy, and L. F. Lester, "Room-temperature operation of InAs quantum-dash lasers on InP [001]," IEEE Photonics Technol. Lett. **13**, 767–769 (2001).

[190]O. Bierwagen and W. T. Masselink, "Self-organized growth of InAs quantum wires and dots on InP(001): The role of vicinal substrates," Appl. Phys. Lett. **86**, 113110 (2005).

[191]J. García, L. González, M. González, J. Silveira, Y. González, and F. Briones, "InAs/InP(001) quantum wire formation due to anisotropic stress relaxation: In situ stress measurements," J. Cryst. Growth **227–228**, 975–979 (2001).

[192]P. J. Simmonds, R. B. Laghumavarapu, M. Sun, A. Lin, C. J. Reyner, B. Liang, and D. L. Huffaker, "Structural and optical properties of InAs/AlAsSb quantum dots with GaAs(Sb) cladding layers," Appl. Phys. Lett. **100**, 243108 (2012).

[193]A. Ponchet, A. Le Corre, H. L'Haridon, B. Lambert, and S. Salaün, "Relationship between self-organization and size of InAs islands on InP (001) grown by gas-source molecular beam epitaxy," Appl. Phys. Lett. **67**, 1850–1852 (1995).

[194]Z. Zhang, Y. Song, Q. Chen, X. Wu, Z. Zhu, L. Zhang, Y. Li, and S. Wang, "Growth mode of tensile-strained Ge quantum dots grown by molecular beam epitaxy," J. Phys. D: Appl. Phys. **50**, 465301 (2017).

[195]J. Bortoleto, A. Gazoto, M. Brasil, E. Meneses, and M. Cotta, "Nucleation and growth evolution of InP dots on InGaP/GaAs," J. Phys. D: Appl. Phys. **43**, 285301 (2010).

[196]J. Bortoleto, H. Gutiérrez, M. Cotta, and J. Bettini, "Mechanism of lateral ordering of InP dots grown on InGaP layers," Appl. Phys. Lett. **87**, 013105 (2005).

[197]J. Bortoleto, H. Gutierrez, M. Cotta, J. Bettini, L. Cardoso, and M. de Carvalho, "Spatial ordering in InP/InGaP nanostructures," Appl. Phys. Lett. **82**, 3523–3525 (2003).

[198]K. Häusler, K. Eberl, F. Noll, and A. Trampert, "Strong alignment of self-assembling InP quantum dots," Phys. Rev. B **54**, 4913 (1996).

[199]W. Jevasuwan, P. Boonpeng, S. Panyakeow, and S. Ratanathammaphan, "Growth and characterization of InP ringlike quantum-dot molecules grown by solid-source molecular beam epitaxy," J. Nanosci. Nanotechnol. **10**, 7291–7294 (2010).

[200]M. Schmidbauer, F. Hatami, M. Hanke, P. Schäfer, K. Braune, W. Masselink, R. Köhler, and M. Ramsteiner, "Shape-mediated anisotropic strain in self-assembled InP/In$_{0.48}$Ga$_{0.52}$P quantum dots," Phys. Rev. B **65**, 125320 (2002).

[201]Y. Wan, D. Jung, J. Norman, C. Shang, I. MacFarlane, Q. Li, M. J. Kennedy, A. C. Gossard, K. M. Lau, and J. E. Bowers, "O-band electrically injected quantum dot micro-ring lasers on on-axis (001) GaP/Si and v-groove Si," Opt. Express **25**, 26853–26860 (2017).

[202]D. Jung, J. Norman, M. Kennedy, C. Shang, B. Shin, Y. Wan, A. C. Gossard, and J. E. Bowers, "High efficiency low threshold current 1.3 μm InAs quantum dot lasers on on-axis (001) GaP/Si," Appl. Phys. Lett. **111**, 122107 (2017).

[203]B. Damilano, N. Grandjean, S. Dalmasso, and J. Massies, "Room-temperature blue-green emission from InGaN/GaN quantum dots made by strain-induced islanding growth," Appl. Phys. Lett. **75**, 3751–3753 (1999).

[204]M. Bürger, J. Lindner, D. Reuter, and D. As, "Investigation of cubic GaN quantum dots grown by the Stranski-Krastanov process," Phys. Status Solidi C **12**, 452–455 (2015).

[205]Ž. Gačević, A. Das, J. Teubert, Y. Kotsar, P. Kandaswamy, T. Kehagias, T. Koukoula, P. Komninou, and E. Monroy, "Internal quantum efficiency of III-nitride quantum dot superlattices grown by plasma-assisted molecular-beam epitaxy," J. Appl. Phys. **109**, 103501 (2011).

[206]T. Schupp, T. Meisch, B. Neuschl, M. Feneberg, K. Thonke, K. Lischka, and D. As, "Growth of cubic GaN quantum dots," AIP Conf. Proc. **1292**, 165–168 (2010).

[207]D. As, S. Potthast, J. Fernandez, J. Schörmann, K. Lischka, H. Nagasawa, and M. Abe, "Ni Schottky diodes on cubic GaN," Appl. Phys. Lett. **88**, 152112 (2006).

[208]S. Blumenthal, D. Reuter, and D. J. As, "Optical properties of cubic GaN quantum dots grown by molecular beam epitaxy," Phys. Status Solidi B **255**, 1700457 (2018).

[209]J. Brault, M. Al Khalfioui, S. Matta, B. Damilano, M. Leroux, S. Chenot, M. Korytov, J. Nkeck, P. Vennéguès, J.-Y. Duboz et al., "UVA and UVB light emitting diodes with Al$_y$Ga$_{1−y}$N quantum dot active regions covering the 305–335 nm range," Semicond. Sci. Technol. **33**, 075007 (2018).

[210]J. Brault, S. Matta, T.-H. Ngo, M. Al Khalfioui, P. Valvin, M. Leroux, B. Damilano, M. Korytov, V. Brändli, P. Vennegues et al., "Internal quantum efficiencies of AlGaN quantum dots grown by molecular beam epitaxy and emitting in the UVA to UVC ranges," J. Appl. Phys. **126**, 205701 (2019).

[211]J. Verma, P. K. Kandaswamy, V. Protasenko, A. Verma, H. Grace Xing, and D. Jena, "Tunnel-injection GaN quantum dot ultraviolet light-emitting diodes," Appl. Phys. Lett. **102**, 041103 (2013).

[212]B. Daudin, F. Widmann, G. Feuillet, Y. Samson, M. Arlery, and J. Rouvière, "Stranski-Krastanov growth mode during the molecular beam epitaxy of highly strained GaN," Phys. Rev. B **56**, R7069 (1997).

[213]X. Wang and A. Yoshikawa, "Molecular beam epitaxy growth of GaN, AlN and InN," Prog. Cryst. Growth Charact. Mater. **48**, 42–103 (2004).

[214]N. Gogneau, D. Jalabert, E. Monroy, T. Shibata, M. Tanaka, and B. Daudin, "Structure of GaN quantum dots grown under "modified Stranski–Krastanow" conditions on AlN," J. Appl. Phys. **94**, 2254–2261 (2003).

[215]F. Tinjod, B. Gilles, S. Moehl, K. Kheng, and H. Mariette, "II–VI quantum dot formation induced by surface energy change of a strained layer," Appl. Phys. Lett. **82**, 4340–4342 (2003).

[216]I. Robin, R. André, H. Mariette, S. Tatarenko, L. S. Dang, J. Bleuse, E. Bellet-Amalric, and J. Gérard, "Control of the two-dimensional–three-dimensional transition of self-organized CdSe/ZnSe quantum dots," Nanotechnology **16**, 1116 (2005).

[217]I.-C. Robin, R. Andre, C. Bougerol, T. Aichele, and S. Tatarenko, "Elastic and surface energies: Two key parameters for CdSe quantum dot formation," Appl. Phys. Lett. **88**, 233103 (2006).

[218]S. Lee, I. Daruka, C. Kim, A.-L. Barabási, J. Merz, and J. Furdyna, "Dynamics of ripening of self-assembled II-VI semiconductor quantum dots," Phys. Rev. Lett. **81**, 3479 (1998).

[219]J. Merz, S. Lee, and J. Furdyna, "Self-organized growth, ripening, and optical properties of wide-bandgap II–VI quantum dots," J. Cryst. Growth **184**, 228–236 (1998).

[220]J. Lee, Z. M. Wang, B. Liang, W. Black, V. P. Kunets, Y. I. Mazur, and G. Salamo, "Selective growth of InGaAs/GaAs quantum dot chains on pre-patterned GaAs (100)," Nanotechnology **17**, 2275 (2006).

[221]I. Daruka and A.-L. Barabási, "Equilibrium phase diagrams for dislocation free self-assembled quantum dots," Appl. Phys. Lett. **72**, 2102–2104 (1998).

[222]M. Rabe, M. Lowisch, and F. Henneberger, "Self-assembled CdSe quantum dots formation by thermally activated surface reorganization," J. Cryst. Growth **184**, 248–253 (1998).

[223]P. Kratzert, M. Rabe, and F. Henneberger, "Self-organized formation of wide-bandgap II–VI quantum dots. Thermally activated surface re-organization versus 2D stabilization," Phys. Status Solidi B **224**, 179–183 (2001).

[224]S. Maćkowski, S. Lee, J. Furdyna, M. Dobrowolska, G. Prechtl, W. Heiss, J. Kossut, and G. Karczewski, "Growth and optical properties of Mn-containing II–VI quantum dots," Phys. Status Solidi B **229**, 469–472 (2002).

[225]E. Kurtz, J. Shen, M. Schmidt, M. Grün, S. Hong, D. Litvinov, D. Gerthsen, T. Oka, T. Yao, and C. Klingshirn, "Formation and properties of self-organized II–VI quantum islands," Thin Solid Films **367**, 68–74 (2000).

[226]P. Wojnar, G. Karczewski, T. Wojtowicz, and J. Kossut, "Changing the properties of the CdTe/ZnTe quantum dots by in situ annealing during the growth," Acta Phys. Pol. A Gen. Phys. **112**, 283–288 (2007).

[227]S. Sorokin, I. Sedova, S. Gronin, G. Klimko, K. Belyaev, M. Rakhlin, I. Mukhin, A. Toropov, and S. Ivanov, "CdTe/Zn(Mg)(Se)Te quantum dots for single photon emitters grown by MBE," J. Cryst. Growth **477**, 127–130 (2017).

[228]S. Sorokin, I. Sedova, K. Belyaev, M. Rakhlin, M. Yagovkina, A. Toropov, and S. Ivanov, "Nanoheterostructures with CdTe/ZnMgSeTe quantum dots for single-photon emitters grown by molecular beam epitaxy," Tech. Phys. Lett. **44**, 267–270 (2018).

[229]A. A. Toropov, O. G. Lyublinskaya, B. Y. Meltser, V. A. Solov'ev, A. A. Sitnikova, M. O. Nestoklon, O. V. Rykhova, S. V. Ivanov, K. Thonke, and R. Sauer, "Tensile-strained GaAs quantum wells and quantum dots in a GaAs$_x$Sb$_{1−x}$ matrix," Phys. Rev. B **70**, 205314 (2004).

[230]B. Y. Meltser, V. Solov'ev, O. Lyublinskaya, A. Toropov, Y. V. Terent'ev, A. Semenov, A. Sitnikova, and S. Ivanov, "Molecular beam epitaxy, photoluminescence and lasing of GaAs/GaSbAs QD nanostructures," J. Cryst. Growth **278**, 119–124 (2005).

[231]T. Taliercio, A. Gassenq, E. Luna, A. Trampert, and E. Tournié, "Highly tensile-strained, type-II, Ga$_{1−x}$In$_x$As/GaSb quantum wells," Appl. Phys. Lett. **96**, 062109 (2010).

[232]A. Lenz, E. Tournié, J. Schuppang, M. Dähne, and H. Eisele, "Atomic structure of tensile-strained GaAs/GaSb(001) nanostructures," Appl. Phys. Lett. **102**, 102105 (2013).

[233]R. Vrijen and E. Yablonovitch, "A spin-coherent semiconductor photodetector for quantum communication," Physica E **10**, 569–575 (2001).

[234]Y. H. Huo, B. J. Witek, S. Kumar, J. R. Cardenas, J. X. Zhang, N. Akopian, R. Singh, E. Zallo, R. Grifone, D. Kriegner, R. Trotta, F. Ding, J. Stangl, V. Zwiller, G. Bester, A. Rastelli, and O. G. Schmidt, "A light-hole exciton in a quantum dot," Nat. Phys. **10**, 46–51 (2013).

[235]H.-S. Lan, S.-T. Chan, T.-H. Cheng, C.-Y. Chen, S.-R. Jan, and C. Liu, "Biaxial tensile strain effects on photoluminescence of different orientated Ge wafers," Appl. Phys. Lett. **98**, 101106 (2011).

[236]M. El Kurdi, G. Fishman, S. Sauvage, and P. Boucaud, "Band structure and optical gain of tensile-strained germanium based on a 30 band k·p formalism," J. Appl. Phys. **107**, 013710 (2010).

[237]H. Tahini, A. Chroneos, R. W. Grimes, U. Schwingenschlögl, and A. Dimoulas, "Strain-induced changes to the electronic structure of germanium," J. Phys.: Condens. Matter **24**, 195802 (2012).

[238]O. Aldaghri, Z. Ikonić, and R. Kelsall, "Optimum strain configurations for carrier injection in near infrared Ge lasers," J. Appl. Phys. **111**, 053106 (2012).

[239]K. D. Vallejo, T. A. Garrett, K. E. Sautter, K. Saythavy, B. Liang, and P. J. Simmonds, "InAs(111)A homoepitaxy with molecular beam epitaxy," J. Vac. Sci. Technol. B **37**, 061810 (2019).

[240]I. Sadeghi, M. C. Tam, and Z. R. Wasilewski, "On the optimum off-cut angle for the growth on InP(111)B substrates by molecular beam epitaxy," J. Vac. Sci. Technol. B **37**, 031210 (2019).

[241]C. D. Yerino, B. Liang, D. L. Huffaker, P. J. Simmonds, and M. L. Lee, "Review Article: Molecular beam epitaxy of lattice-matched InAlAs and InGaAs layers on InP(111)A, (111)B, and (110)," J. Vac. Sci. Technol. B **35**, 010801 (2017).

[242]C. F. Schuck, "(111)-oriented gallium arsenide tensile-strained quantum dots tailored for entangled photon emission," Ph.D. dissertation (Boise State University, 2019).

[243]C. Yang, Z. Yu, Y. Liu, P. Lu, T. Gao, M. Li, and S. Manzoor, "Dependence of electronic properties of germanium on the in-plane biaxial tensile strains," Physica B **427**, 62–67 (2013).

[244]J. Zide, A. Kleiman-Shwarsctein, N. Strandwitz, J. Zimmerman, T. Steenblock-Smith, A. Gossard, A. Forman, A. Ivanovskaya, and G. Stucky, "Increased efficiency in multijunction solar cells through the incorporation of semimetallic eras nanoparticles into the tunnel junction," Appl. Phys. Lett. **88**, 162103 (2006).

[245]W. Kim, J. Zide, A. Gossard, D. Klenov, S. Stemmer, A. Shakouri, and A. Majumdar, "Thermal conductivity reduction and thermoelectric figure of merit increase by embedding nanoparticles in crystalline semiconductors," Phys. Rev. Lett. **96**, 045901 (2006).

[246]A. M. Crook, H. P. Nair, and S. R. Bank, "High-performance nanoparticle-enhanced tunnel junctions for photonic devices," Phys. Status Solidi C **7**, 2544–2547 (2010).

[247]M. Zhao, X. Chen, L. Li, and X. Zhang, "Driving a GaAs film to a large-gap topological insulator by tensile strain," Sci. Rep. **5**, 8441 (2015).

[248]Y. Huo, H. Lin, R. Chen, Y. Rong, T. I. Kamins, and J. S. Harris, "MBE growth of tensile-strained Ge quantum wells and quantum dots," Front. Optoelectron. **5**, 112–116 (2012).

[249]D. Pachinger, H. Groiss, H. Lichtenberger, J. Stangl, G. Hesser, and F. Schäffler, "Stranski-Krastanow growth of tensile strained Si islands on Ge (001)," Appl. Phys. Lett. **91**, 233106 (2007).